Orbital stabilization of an underactuated bipedal gait via nonlinear H ∞ -control using measurement feedback

Oscar Montano, Yury Orlov, Yannick Aoustin, Christine Chevallereau

Noname manuscript No.
(will be inserted by the editor)

Orbital stabilization of an underactuated bipedal gait via nonlinear $\mathcal{H}_\infty$-control using measurement feedback

Oscar Montano · Yury Orlov · Yannick Aoustin · Christine Chevallereau

Received: date / Accepted: date

Abstract The primary concern of the work is robust control of hybrid mechanical systems under unilateral constraints with underactuation degree one. Nonlinear $\mathcal{H}_\infty$ output feedback synthesis is developed in the hybrid setting, covering collision phenomena. Sufficient conditions are presented to ensure internal asymptotic stability while also attenuating external disturbances and plant uncertainties. The developed synthesis is applied to the orbital stabilization of an underactuated bipedal robot periodically touching the ground. Good performance of the closed-loop system is obtained not only in the presence of measurement noise and external disturbances, affecting the gait of the biped between collision time instants, but also under uncertainties at the velocity restitution when the ground collision occurs.

Keywords robust control · unilateral constraints · underactuated mechanical systems · orbital stabilization · bipedal robot · walking gait.

1 Introduction

Significant research interest has recently been attracted to hybrid dynamical systems due to the wide variety of their applications and due to the need of special analysis tools for this type of systems (see, e.g., the relevant works of Goebel et al (2009); Hamed and Grizzle (2013); Naldi and Sanfelice (2013); Nešić et al (2013), and references quoted therein). Particularly, the disturbance attenuation problem for hybrid dynamical systems has been addressed in, for example, the works by Haddad et al (2005) and Nešić et al (2008, 2013) where impulsive control inputs were admitted to counteract/compensate disturbances/uncertainties at time instants of instantaneous changes of the underlying state. It should be noted, however, that even in the state feedback design, a pair of independent Riccati equations, separately coming from continuous and discrete dynamics, was required to possess a solution that satisfies both equations, thus yielding a restrictive condition on the feasibility of the proposed synthesis. Moreover, the physical implementation of impulsive control inputs remains impossible in many practical situations, e.g., while controlling walking biped robots.

Other robust control techniques, such as sliding modes control, have been designed for this kind of systems (see *e.g.*, the works by Raibert et al (1993), Manamani et al (1997), Nikkhah et al (2007), Aoustin et al (2010), Oza et al (2014). While providing both finite-time convergence to a desired reference trajectory and disturbance rejection, these approaches also entail the well-known problem of chattering in the actuators.

Stability of bipedal locomotion has been a recent topic of research. For example, in the work by Westervelt et al (2004), the authors stabilized a planar underactuated biped around a periodic orbit, but instead of a sliding mode or finite-time converging controller, the authors preferred to use a decoupled PD control law for its robustness to noise. Hamed et al (2014) proposed a control strategy to exponentially stabilize an underactuated biped using a time-invariant continuous-time controller; however, the effects of external distur-

O. Montano, Y. Orlov
CICESE, Carretera Ensenada-Tijuana No. 3918, Zona Playitas, C.P. 22860, Ensenada, B.C. Mexico.
Tel.: +52-686-1750500
E-mail: omontano@cicese.edu.mx, yorlov@cicese.mx

Y. Aoustin, C. Chevallereau
L'IRCCyN, 1, rue de la Noe, BP 92101, 44321 NANTES Cedex 3
E-mail: {yannick.aoustin, christine.chevallereau}@irccyn.ec-nantes.fr

bances were not explicitly taken into account for the synthesis of the controller, and a perfect knowledge of the complete state vector was assumed. In the works by Chevallereau et al (2009) and Hamed and Grizzle (2014), event based controllers were developed to robustly stabilize periodic orbits for underactuated biped systems. Also, based on the Poincaré map, Hobbelen and Wisse (2007) introduced the gait sensitivity norm as a measure of the robustness cycle limits in bipedal walkers. Miossec and Aoustin (2005) inserted a double support to reinforce the stability of the walking gait of an underactuated biped and studied the stability of the dynamics not controlled during the single support phase, considering a perfect tracking of the references of the other joint angles of the biped.

In this regard, two major drawbacks should be mentioned with the methods based on the Poincaré map analysis. On one hand, it is hardly possible to include uncertainties into the free-motion phase, since the analysis is made only on the selected Poincaré section. On the other hand, it is difficult to represent the Poincaré map in the closed form since it relies on finding the analytical solution to the differential equations that describe the motion of the system. As stated by Morris and Grizzle (2005), numerical schemes can be used to compute the return map, to find its fixed points, and to estimate eigenvalues for determining exponential stability. However, the numerical computations are usually time-intensive, and performing them iteratively as part of a system design process can be cumbersome. A more important drawback is that numerical computations are not insightful for a fixed point of the Poincaré map to exist and to possess desired stability properties as these computations, made *a priori*, do not allow one to tune the controller gains in the closed loop.

The orbital stability analysis has recently been addressed using the moving Poincaré section approach (Leonov, 2006). In contrast to the standard Poincaré analysis, dealing with a single transversal surface at a fixed point, the moving Poincaré section method involves a family of transversal surfaces at each point on the cyclic trajectory. The linearized dynamics on the foliation of these surfaces are governed by a linear time-varying and periodic system, whose dimension is less than the original system by one. Therefore, asymptotic orbital stability of the desired motion can be studied by analyzing the stability of this auxiliary transversal system. Coupled to the virtual holonomic constraint approach, the transverse linearization has proved to be a powerful method for orbital stabilization around desired periodic motions (see the works by Shiriaev et al (2008); Freidovich et al (2008); Shiriaev and Freidovich (2009); La Hera et al (2013) and references cited therein).

Thus motivated, this investigation is devoted to the derivation of sufficient conditions for a new output feedback control strategy, that would result in the asymptotic orbital stabilization of the undisturbed hybrid system of interest, while also guaranteing the $\mathcal{L}_2$-gain of its disturbed version to be less than an appropriate disturbance attenuation level γ. The work focuses on impulse hybrid systems, recognized as dynamical systems under unilateral constraints (Brogliato, 1999). Since the dynamic systems with unilateral constraints possess nonsmooth solutions, which arise due to hitting the constraints, a challenging problem is to extend the popular nonlinear $\mathcal{H}_\infty$ approach (see the works by Van Der Schaft (1991), Isidori and Astolfi (1992), and Basar and Bernhard (1995)) to this kind of dynamic systems.

The $\mathcal{H}_\infty$ approach, that has recently been developed by Orlov and Aguilar (2014) towards nonsmooth mechanical applications with hard-to-model friction forces (such as dry or Coulomb friction and backlash effects), and then extended by Montano et al (2014) to fully actuated systems under unilateral constraints, is now generalized to an underactuated mechanical system with collisions. As in the fully actuated case (Montano et al, 2014), a local synthesis of an underactuated system is derived in the presence of unilateral constraints by means of two coupled Riccati equations that appear in solving the $\mathcal{H}_\infty$ state feedback and output injection designs for the linearized system viewed beyond the system constraints.

An essential feature, adding value to the present investigation, is that standard external disturbances (such as environmental external forces, biped parameters uncertainty, etc.), their discrete-time counterparts (such as non-perfect inelastic contact between the floor and the foot at the impact, or floor height variations), and measurement imperfections are considered in combination and are attenuated with the proposed synthesis. This in contrast to the existing literature where the perfect knowledge of both the state vector, and of the impact equation at the collision time instants is assumed.

In order to illustrate capabilities of the proposed synthesis it is further developed to the orbital stabilization of an underactuated planar bipedal robot under ground unilateral constraints and subject to external disturbances in the over-all hybrid dynamical system. Due to the existence of a free-motion and a transition phase, the bipedal robot represents a hybrid system whose desired orbit to track is actually required to be attained at a sufficiently rapid rate, before occurring the next contact between the swing leg and the ground (Morris and Grizzle, 2005). The underactuation degree

of the robot is one during the single support phase. The effects of the disturbances during the single support phase and during the impact phase are studied.

In the recent work of Dai and Tedrake (2012) and Dai and Tedrake (2013), a hybrid $\mathcal{H}_\infty$ control approach was developed by defining an $\mathcal{L}_2$-gain from ground perturbations to deviations from the nominal limit cycle. In contrast to the work of Dai and Tedrake (2013), the present work demonstrates good robustness features of the developed orbital synthesis against both external disturbances, affecting the collision-free motion phase, and against uncertainties that occur in the collision phase, while using only the available measurements of the plant variables. Along with the theoretical development of the nonsmooth orbital $\mathcal{H}_\infty$ synthesis under unilateral constraints, these robustness features, numerically justified on a biped emulator (Aoustin et al, 2010), form the novelty of the paper.

The contribution, this paper makes into the existing literature, is thus twofold. First, the nonlinear $\mathcal{H}_\infty$ approach is constructively generalized to position feedback tracking of underactuated mechanical systems, operating under unilateral constraints. Second, the resulting synthesis is then effectively applied to the orbital stabilization of underactuated mechanical systems with collisions to demonstrate good robustness features against external disturbances in the collision-free phase, uncertainties in the collision phase, and disturbances in the position measurements.

The paper is outlined as follows. Section 2 presents a hybrid model of interest which is subject to an unilateral constraint. Background materials on $\mathcal{H}_\infty$-control, virtual constraints, and transversal coordinates are presented in Section 3. A locally stabilizing nonlinear $\mathcal{H}_\infty$ controller is synthesized in Section 4. This controller is then generalized in Section 5 for an underactuated biped, walking in the saggital plane, and its capabilities are illustrated in simulation runs made on an emulator. Finally, conclusions and potential extensions of this work are collected in Section 6.

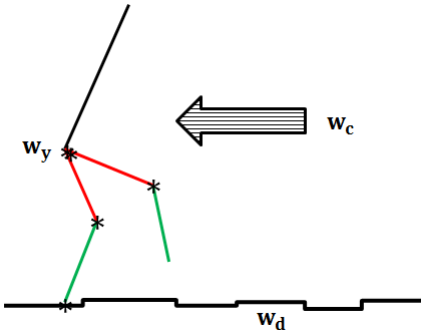

Fig. 1 Disturbances present in bipedal locomotion

1.1 Notation

The notation used throughout is rather standard. The variable $\mathbf{x}^+$ is used to denote the post-impact value $\mathbf{x}(t_i^+)$ of a trajectory $\mathbf{x}(t_i)$ at an impact time instant t_i whereas $\mathbf{x}^-$ stands for the pre-impact value of the same; by default, $\mathbf{x}(t)$ is reserved for $\mathbf{x}^-$, thus implying an underlying trajectory to be continuous on the left.

2 Objective

Given a scalar unilateral constraint $F(q) \geq 0$ of class C^1, consider a nonlinear system, evolving within the above constraint, which is governed by continuous dynamics of the form

$$\mathbf{D}(\mathbf{q})\ddot{\mathbf{q}} + \mathbf{C}(\mathbf{q}, \dot{\mathbf{q}})\dot{\mathbf{q}} + \mathbf{G}(\mathbf{q}) = \mathbf{B}\boldsymbol{\Gamma} + \mathbf{w_c} \tag{1}$$

out of the surface $F(q) = 0$ when the constraint is inactive, and by the algebraic relations

$$\begin{bmatrix} \mathbf{q}^+ \\ \dot{\mathbf{q}}^+ \end{bmatrix} = \mu(\mathbf{q}^-, \dot{\mathbf{q}}^-) + \boldsymbol{\omega}(\mathbf{q}^-, \dot{\mathbf{q}}^-)\mathbf{w_d} \tag{2}$$

when the system trajectory hits the surface $F(q) = 0$. The vectors $\mathbf{q} \in \mathbb{R}^n$ and $\dot{\mathbf{q}} \in \mathbb{R}^n$ are generalized positions and velocities, respectively, $\mathbf{D}$ is a $n \times n$ symmetric, positive definite inertia matrix, $\mathbf{B}$ is a $n \times (n-k)$ constant matrix composed of 0 and 1 which defines the underactuated and the actuated variables, whereas $\boldsymbol{\Gamma} \in \mathbb{R}^{n-k}$ with $1 \leq k < n$ is the vector of actuated torques (thus covering underactuated systems); μ represents the impact equation; $\mathbf{w_c} \in \mathbb{R}^n$ represents external disturbances affecting the continuous dynamics, whereas $\mathbf{w_d} \in \mathbb{R}^s$ represents disturbances affecting the impact equation (2) (see Fig. 1). The vector $\mathbf{C}(\mathbf{q}, \dot{\mathbf{q}})\dot{\mathbf{q}}$ stands for centrifugal and Coriolis forces whereas $\mathbf{G}(\mathbf{q})$ stands for the gravity forces. This work will focus in mechanical systems of underactuation degree 1 during their locomotion, so $k = 1$.

Let us consider that a certain task is achieved by carrying out a feasible trajectory $\mathbf{q}_\star$ of the hybrid mechanical system (1)-(2), and this feasible trajectory will describe a periodic orbit, given by

$$\mathcal{O}_\star = \{(\mathbf{q}, \dot{\mathbf{q}}) \in \mathbb{R}^{2n} : \mathbf{q} = \mathbf{q}_\star(\theta), \dot{\mathbf{q}} = \dot{\mathbf{q}}_\star(\theta, \dot{\theta})\} \tag{3}$$

where θ is called a phasing variable, and is a scalar quantity, which is strictly monotonic on the periodic orbit. Let $\theta_\star$ denote the evolution of θ corresponding to the periodic orbit $\mathcal{O}_\star$, then $\theta_\star|_t = \theta_\star|_{(t+T_s)}$, where $T_s > 0$ stands for the period of the motion.

As presented in the work of Hamed et al (2014), now lets consider a controller $\boldsymbol{\Gamma}$ of the form

$$\boldsymbol{\Gamma} = \boldsymbol{\Gamma}_\star + \mathbf{u}, \tag{4}$$

where $\mathbf{\Gamma}_\star$ is a feedforward term corresponding to the periodic orbit $\mathcal{O}_\star$, and $\mathbf{u}$ is a feedback control law that internally stabilizes the closed-loop system system (1)-(2) to a feasible trajectory $\mathbf{q}_\star(\theta)$. Thus the existence of the periodic orbit $\mathcal{O}_\star$ as well as the existence of the feedforward term $\mathbf{\Gamma}_\star$ are postulated *a priori*.

Therefore, the orbital stabilization problem in question is to find an appropriate control action $\mathbf{\Gamma}$ such that the solutions of the undisturbed version of(1), (2), initiated in a neighborhood of the desired orbit $\mathcal{O}_\star$, defined by (3), asymptotically approach the compact set $\mathcal{O}_\star$, and for the disturbed version, attenuate the effect of the disturbances on the continuous dynamics (1) and the restitution law (2).

3 Background Materials

In this section, sufficient conditions of a fully actuated hybrid system (formally corresponding to the case $k = 0$) to possess a solution to the attenuation problem are first recalled from Montano et al (2014, 2015a). Then, the virtual holonomic constraint approach is presented as well as the concepts of transverse coordinates and transverse linearization are. Coupled together, these results form a basis of attenuating disturbances in mechanical systems of underactuation degree one ($k = 1$).

3.1 The $\mathcal{H}_\infty$-Control Problem

Consider the nonlinear hybrid system

$$\begin{aligned} \dot{\mathbf{x}} &= \mathbf{f}(\mathbf{x},t) + \mathbf{g_1}(\mathbf{x},t)\mathbf{w_c} + \mathbf{g_2}(\mathbf{x},t)\mathbf{u}, \quad F(\mathbf{x_1},t) > 0 \\ \mathbf{x}^+ &= \mathbf{\Delta}(\mathbf{x}^-,t) + \boldsymbol{\omega}(\mathbf{x}^-,t)\mathbf{w_d}, \quad F(\mathbf{x_1},t) = 0 \end{aligned} \tag{5}$$

where $\mathbf{x} = [\mathbf{x_1}, \mathbf{x_2}]^\top \in \mathbb{R}^{2n}$ is the state vector and $\mathbf{u} \in \mathbb{R}^n$ is the control input; $\mathbf{f}(\mathbf{x},t)$, $\mathbf{g_1}(\mathbf{x},t)$ and $\mathbf{g_2}(\mathbf{x},t)$ are continuously differentiable in their arguments and uniformly bounded in t. In addition, the origin is assumed to be an equilibrium of the unforced and undisturbed system (5), i.e., for all t and $\mathbf{u} = \mathbf{w_c} = \mathbf{w_d} = \mathbf{0}$, one has $\mathbf{f}(\mathbf{0},t) = \mathbf{0}$ and $\mathbf{\Delta}(\mathbf{0},t) = \mathbf{0}$. Assuming that only position measurements are available, the outputs to be controlled (driven to zero) can be defined as

$$\mathbf{z} = \mathbf{h_1}(\mathbf{x},t) + \mathbf{k_{12}}(\mathbf{x},t)\mathbf{u} \tag{6}$$

for the dynamics between impacts (which is the standard form for the controlled output in the impact-less time-varying case, see for *e.g.* (Orlov et al, 1999)), and

$$\mathbf{z_i^d} = \mathbf{x}^+ \tag{7}$$

for the dynamics at the impact instants, with variables $\mathbf{z} \in \mathbb{R}^m$ and $\mathbf{z_i^d} \in \mathbb{R}^n$, whereas

$$\mathbf{y} = \mathbf{h_2}(\mathbf{x},t) + \mathbf{k_{21}}(\mathbf{x},t)\mathbf{w_y} \tag{8}$$

with $\mathbf{y} \in \mathbb{R}^p$, $p \geq n$, is the only available measurement of the state of the system; $\mathbf{w_y}$ represents the disturbances in the measurements; also, for all t, $\mathbf{h_1}(\mathbf{0},t) = \mathbf{0}$, $\mathbf{h_2}(\mathbf{0},t) = \mathbf{0}$. In order to simplify the synthesis to be developed and to provide reasonable expressions for the controller design, the following assumptions

$$\begin{aligned} &\mathbf{h_1}^\top \mathbf{k_{12}} = \mathbf{0},\ \mathbf{k_{12}}^\top \mathbf{k_{12}} = \mathbf{I}, \\ &\mathbf{k_{21}}\mathbf{g_1}^\top = \mathbf{0},\ \mathbf{k_{21}}\mathbf{k_{21}}^\top = \mathbf{I}, \end{aligned} \tag{9}$$

which are standard in the literature (Isidori and Astolfi, 1992), are made. The first and second ones mean that in the norm of the output variable $\mathbf{z}$ there is no cross product involving $\mathbf{h_l}(\mathbf{x},t)$ and input $\mathbf{u}$ and that the control weight matrix is the identity. The third and fourth ones are dual to the first and second ones. Relaxing these assumptions is indeed possible, but it would substantially complicate the formulas to be worked out.

For later use, the notion of an admissible controller is specified for the underlying system. Consider a causal dynamic feedback controller of the same structure

$$\begin{aligned} \dot{\boldsymbol{\xi}} = \boldsymbol{\eta}(\boldsymbol{\xi},\mathbf{y},t) \quad \boldsymbol{\xi}^+ &= \mathbf{\Delta}_\xi(\boldsymbol{\xi}^-,t) \\ \mathbf{u} &= \boldsymbol{\kappa}(\boldsymbol{\xi},t) \end{aligned} \tag{10}$$

as that of the plant and with the internal state $\boldsymbol{\xi} = [\boldsymbol{\xi}_1, \boldsymbol{\xi}_2]^\top \in \mathbb{R}^{2n}$, representing the state estimation of $\mathbf{x}$, with the time instants $t = t_j,\ j = 1,2,\ldots$, which are not necessarily coinciding with the collision time instants in the plant equations (5), and with uniformly bounded in t functions $\boldsymbol{\eta}(\boldsymbol{\xi},\mathbf{y},t)$, $\mathbf{\Delta}_\xi(\boldsymbol{\xi},t)$, and $\boldsymbol{\kappa}(\boldsymbol{\xi},t)$ of class C^1 such that $\boldsymbol{\eta}(\mathbf{0},t) = \mathbf{0}$, $\mathbf{\Delta}_\xi(\mathbf{0},t) = \mathbf{0}$, and $\boldsymbol{\kappa}(\mathbf{0},t) = \mathbf{0}$ for all t. Such a controller is said to be a locally *admissible controller* iff the undisturbed closed-loop system (5), (10) with $\mathbf{w_c}$, $\mathbf{w_y}$, $\mathbf{w_d} = \mathbf{0}$ is uniformly asymptotically stable, thus driving the controlled outputs (6) and (7) to zero.

The $\mathcal{H}_\infty$-control problem of interest consists in finding a locally admissible controller (if any) such that the $\mathcal{L}_2$-gain of the disturbed system is less than a certain $\gamma > 0$, that is the inequality (Montano et al, 2014)

$$\begin{aligned} &\int_{t_0}^{T} \|\mathbf{z}(t)\|^2 \mathrm{d}t + \sum_{i=1}^{N_T} \|\mathbf{z_i^d}\|^2 \leq \\ &\gamma^2 \left[\int_{t_0}^{T} \|\mathbf{w}(t)\|^2 \mathrm{d}t + \sum_{i=1}^{N_T} \|\mathbf{w_{d_i}}\|^2 \right] \\ &\qquad + \sum_{k=0}^{N_T} \beta_k(\mathbf{x}(t_k^-), \boldsymbol{\xi}(t_k^-), t_k) \end{aligned} \tag{11}$$

holds for some positive definite functions $\beta_k(\mathbf{x},\boldsymbol{\xi},t)$, $k=0,\dots,N_T$, for all segments $[t_0,T]$ and a natural N_T such that $t_{N_T}\le T<t_{N_T+1}$, for all piecewise continuous disturbances $\mathbf{w}=[\mathbf{w_y}^\top,\mathbf{w_c}^\top]^\top$ and discrete ones $\mathbf{w_{d_i}}$, $i=1,2,\dots$, for which the state trajectory of the closed-loop system starting from an initial point $(\mathbf{x}(t_0),\boldsymbol{\xi}(t_0))=(\mathbf{x_0},\boldsymbol{\xi_0})\in\mathcal{U}$ remains in some neighborhood $\mathcal{U}\in\mathbb{R}^{4n}$ of the origin for all $t\in[t_0,T]$. This means that the influence of the disturbances $\mathbf{w}$ and $\mathbf{w_{d_i}}$ is attenuated on the outputs $\mathbf{z}$ and $\mathbf{z_d}$.

3.2 $\mathcal{H}_\infty$-Output Feedback Synthesis Under Unilateral Constraints

Let us consider the $\mathcal{H}_\infty$ control problem for the linearized system which is given by

$$\dot{\mathbf{x}}=\mathbf{A}(t)\mathbf{x}+\mathbf{B_1}(t)\mathbf{w}+\mathbf{B_2}(t)\mathbf{u}, \tag{12}$$
$$\mathbf{z}=\mathbf{C_1}(t)\mathbf{x}+\mathbf{D_{12}}(t)\mathbf{u}, \tag{13}$$
$$\mathbf{y}=\mathbf{C_2}(t)\mathbf{x}+\mathbf{D_{21}}(t)\mathbf{w}, \tag{14}$$

within impact-free time intervals (t_{i-1},t_i) where t_0 is the initial time instant and t_i, $i=1,2,\dots$ are the collision time instants whereas

$$\mathbf{A}(t)=\left.\frac{\partial\mathbf{f}}{\partial\mathbf{x}}\right|_{\mathbf{x=0}},\ \mathbf{B_1}(t)=\mathbf{g_1}(0,t),\quad \mathbf{B_2}(t)=\mathbf{g_2}(0,t),$$
$$\mathbf{C_1}(t)=\left.\frac{\partial\mathbf{h_1}}{\partial\mathbf{x}}\right|_{\mathbf{x=0}},\ \mathbf{D_{12}}(t)=\mathbf{k_{12}}(0,t),$$
$$\mathbf{C_2}(t)=\left.\frac{\partial\mathbf{h_2}}{\partial\mathbf{x}}\right|_{\mathbf{x=0}},\ \mathbf{D_{21}}(t)=\mathbf{k_{21}}(0,t). \tag{15}$$

By the time-varying strict bounded real lemma (Orlov and Aguilar, 2014, p.46), the following conditions are necessary and sufficient for the linear $\mathcal{H}_\infty$ control problem (12)-(14) to possess a solution: given $\gamma>0$,

C1) there exists a positive constant ε_0 such that the differential Riccati equation

$$-\dot{\mathbf{P}}_\varepsilon(t)=\mathbf{P}_\varepsilon(t)\mathbf{A}(t)+\mathbf{A}^\top(t)\mathbf{P}_\varepsilon(t)+\mathbf{C_1}^\top(t)\mathbf{C_1}(t)$$
$$+\mathbf{P}_\varepsilon(t)[\frac{1}{\gamma^2}\mathbf{B_1}\mathbf{B_1}^\top-\mathbf{B_2}\mathbf{B_2}^\top](t)\mathbf{P}_\varepsilon(t)+\varepsilon\mathbf{I} \tag{16}$$

has a uniformly bounded symmetric positive definite solution $\mathbf{P}_\varepsilon(t)$ for each $\varepsilon\in(0,\varepsilon_0)$;

C2) while being coupled to (16), the differential Riccati equation

$$\dot{\mathbf{Z}}_\varepsilon(t)=\mathbf{A}_\varepsilon(t)\mathbf{Z}_\varepsilon(t)+\mathbf{Z}_\varepsilon(t)\mathbf{A}_\varepsilon^\top(t)+\mathbf{B_1}(t)\mathbf{B_1}^\top(t)$$
$$+\mathbf{Z}_\varepsilon(t)[\frac{1}{\gamma^2}\mathbf{P}_\varepsilon\mathbf{B_2}\mathbf{B_2}^\top\mathbf{P}_\varepsilon-\mathbf{C_2}^\top\mathbf{C_2}](t)\mathbf{Z}_\varepsilon(t)+\varepsilon\mathbf{I}, \tag{17}$$

has a uniformly bounded symmetric positive definite solution $\mathbf{Z}_\varepsilon(t)$ with

$$\mathbf{A}_\varepsilon(t)=\mathbf{A}(t)+\frac{1}{\gamma^2}\mathbf{B_1}(t)\mathbf{B_1}^\top(t)\mathbf{P}_\varepsilon(t).$$

In order to insure dissipation at the impact times, the following conditions are also considered:

C3) the norm of the matrix function $\boldsymbol{\omega}$ (see (5)) is upper bounded by $\frac{\sqrt{2}}{2}\gamma$, i.e.,

$$\|\boldsymbol{\omega}(\mathbf{x},t)\|\le\frac{\sqrt{2}}{2}\gamma. \tag{18}$$

C4) the functions $V(\mathbf{x},t)=\mathbf{x}^\top\mathbf{P}_\varepsilon(t)\mathbf{x}$ and $W(\mathbf{x},\boldsymbol{\xi},t)=\gamma^2(\mathbf{x}-\boldsymbol{\xi})^\top\mathbf{Z}_\varepsilon^{-1}(t)(\mathbf{x}-\boldsymbol{\xi})$ decrease along the direction $\boldsymbol{\mu}$ in the sense that the inequalities

$$V(\mathbf{x},t)\ge V(\boldsymbol{\Delta}(\mathbf{x},t),t), \tag{19}$$
$$W(\mathbf{x},\boldsymbol{\xi},t)\ge W(\boldsymbol{\Delta}(\mathbf{x},t),\boldsymbol{\Delta}(\boldsymbol{\xi},t),t) \tag{20}$$

hold in the domains of V and W.

Under these conditions, the following theorem is presented.

Theorem 1 *(Montano et al, 2015a) Let conditions C1)-C4) be satisfied with some $\gamma>0$. Then the closed-loop* (5)-(7) *system driven by the output feedback*

$$\dot{\boldsymbol{\xi}}=\mathbf{f}(\boldsymbol{\xi},t)+\mathbf{Z}_\varepsilon\mathbf{C_2}^\top(t)[\mathbf{y}-\mathbf{h_2}(\boldsymbol{\xi},t)]$$
$$+\left[\frac{1}{\gamma^2}\mathbf{g_1}(\boldsymbol{\xi},t)\mathbf{g_1}^\top(\boldsymbol{\xi},t)-\mathbf{g_2}(\boldsymbol{\xi},t)\mathbf{g_2}^\top(\boldsymbol{\xi},t)\right]\mathbf{P}_\varepsilon(t)\boldsymbol{\xi} \tag{21}$$
$$\boldsymbol{\xi}^+=\boldsymbol{\Delta}(\boldsymbol{\xi}^-,t_i)$$
$$\mathbf{u}=-\mathbf{g_2}(\boldsymbol{\xi},t)^\top\mathbf{P}_\varepsilon(t)\boldsymbol{\xi} \tag{22}$$

locally possesses a $\mathcal{L}_2$-gain less than γ. Moreover, the disturbance-free closed-loop system (5)-(7), (21)-(22) *is uniformly asymptotically stable.*

Thus, the synthesized controller will consist of a robust state estimator (21), providing disturbance attenuation for the non-perfect position measurements, and the robust control law (22), locally attenuating the disturbances around the desired trajectory.

For autonomous systems, all functions in (5)-(8) and (15) are time-independent, and the differential Riccati equations (16) and (17) degenerate to the algebraic Riccati equations with $\dot{\mathbf{P}}_\varepsilon(t)=0$ and $\dot{\mathbf{Z}}_\varepsilon(t)=0$.

For periodic systems of period T with periodic impact instants $t_{i+1}=t_i+T$, $i=1,2,\dots$, all functions in (5)-(8) and (15) are time-periodic, and Theorem 1 admits a time-periodic synthesis (21)-(22) which is based on appropriate periodic solutions $\mathbf{P}_\varepsilon(t)$ and $\mathbf{Z}_\varepsilon(t)$ to the periodic differential Riccati equations (16) and (17). It

should be noted that just in case, $P_\varepsilon(t_{i+1}^+) = P_\varepsilon(t_i^+)$, $Z_\varepsilon(t_{i+1}^+) = Z_\varepsilon(t_i^+)$ due to the periodicity, and conditions (19), (20) of Hypothesis H4) are then specified to the boundary conditions

$$\mathbf{x}^\top \mathbf{P}_\varepsilon(t_2^-)\mathbf{x} \geq \boldsymbol{\Delta}^\top(\mathbf{x}, t_1^+))\mathbf{P}_\varepsilon(t_1^+)\boldsymbol{\Delta}^\top(\mathbf{x}, t_1^+)), \tag{23}$$

$$(\mathbf{x}-\xi)^\top \mathbf{Z}_\varepsilon(t_2^-)(\mathbf{x}-\xi) \geq [\boldsymbol{\Delta}(\mathbf{x}, t_1^+) - \boldsymbol{\Delta}(\xi, t_1^+)]^\top \mathbf{Z}_\varepsilon(t_1^+)[\boldsymbol{\Delta}(\mathbf{x}, t_1^+) - \boldsymbol{\Delta}(\xi, t_1^+)] \tag{24}$$

on the Riccati equations (16), (17). The need of such boundary relations on the Riccati equations has been recognized in the literature for the correct generation of periodic biped locomotion (cf. inequality (39) of La Hera et al (2013)).

For the full information case, the controller to be synthesized is a particular case of the previous one, and it is presented below.

Theorem 2 *(Montano et al, 2014) Let conditions C1), C3) and* (19) *be satisfied with some* $\gamma > 0$. *Then the closed-loop* (5)-(7) *system driven by the output feedback*

$$\mathbf{u} = -\mathbf{g_2}(\mathbf{x}, t)^\top \mathbf{P}_\varepsilon(t)\mathbf{x} \tag{25}$$

locally possesses a $\mathcal{L}_2$*-gain less than* γ. *Moreover, the disturbance-free closed-loop system* (5)-(7), (25) *is uniformly asymptotically stable.*

While these results are valid for fully-actuated mechanical systems under unilateral constraints, additional considerations, required for the orbital stabilization synthesis of the underactuated mechanical system of interest, is presented next.

3.3 Virtual Constraint Approach and Transverse Coordinates

The virtual holonomic constraint (VHC) approach is a powerful analytical tool of planning periodic motions in underactuated mechanical systems . Along with the system representation (1)-(2) in the generalized coordinates

$$q_1 = q_1(t), \ldots, q_n = q_n(t), \quad t \in [0, T_s], \tag{26}$$

an alternative time independent representation can be given in the parametric form

$$q_1 = \phi_1(\theta), \ldots, q_n = \phi_n(\theta), \quad \theta \in [\theta_0, \theta_f] \tag{27}$$

to be valid along a desired orbit, specified with functions $\phi_i(\cdot)$, $i = 1, \ldots, n$, which are functions of a parameter θ. Identities (27) are known as virtual holonomic constraints since they express algebraic relations among the generalized coordinates. The parameter θ can be chosen as one of the generalized coordinates (Shiriaev et al, 2005) or as a linear combination of them (Westervelt et al, 2007).

The dynamics of (1) in the new coordinates (27) can now be obtained by introducing the time derivatives $\dot{q}_i = \phi_i'\dot{\theta}$, $\ddot{q}_i = \phi_i''\dot{\theta}^2 + \phi_i'\ddot{\theta}$, $i = 1, \ldots, n$ into the Euler-Lagrange equation (1), where $\phi_i' = \frac{\partial \phi_i}{\partial \theta}$ and $\phi_i'' = \frac{\partial^2 \phi_i}{\partial \theta^2}$. The resulting equation is then governed by

$$\mathbf{D}(\mathbf{\Phi}(\theta))\left[\mathbf{\Phi}'(\theta)\ddot{\theta} + \mathbf{\Phi}''\dot{\theta}^{\mathbf{2}}\right] + \mathbf{C}\left(\mathbf{\Phi}(\theta), \mathbf{\Phi}'(\theta)\dot{\theta}\right)\mathbf{\Phi}'(\theta)\dot{\theta}^{\mathbf{2}} + \mathbf{G}(\mathbf{\Phi}(\theta)) = \mathbf{B}(\mathbf{\Phi}(\theta))\mathbf{\Gamma} \tag{28}$$

where

$$\mathbf{\Phi}(\theta) = [\phi_1(\theta), \ldots, \phi_n(\theta)]^\top \tag{29}$$

$$\mathbf{\Phi}'(\theta) = [\phi_1'(\theta), \ldots, \phi_n'(\theta)]^\top \tag{30}$$

$$\mathbf{\Phi}''(\theta) = [\phi_1''(\theta), \ldots, \phi_n''(\theta)]^\top. \tag{31}$$

Since the present development is confined to mechanical systems (1) of underactuation degree 1, there exists a nontrivial matrix function $\mathbf{B}^\perp(q) \in \mathbb{R}^{1\times n}$ such that $\mathbf{B}^\perp(\mathbf{q})\mathbf{B}(\mathbf{q}) = \mathbf{0}$. Therefore, multiplying (28) by $\mathbf{B}^\perp(\mathbf{q})$ from the left, one arrives at the reduced second order dynamics along the holonomic constraints (27):

$$\bar{\alpha}(\theta)\ddot{\theta} + \bar{\beta}(\theta)\dot{\theta}^2 + \bar{\gamma}(\theta) = 0 \tag{32}$$

where

$$\bar{\alpha}(\theta) = \mathbf{B}^\perp(\mathbf{\Phi}(\theta))\mathbf{D}(\mathbf{\Phi}(\theta))\mathbf{\Phi}'(\theta) \tag{33}$$

$$\bar{\beta}(\theta) = \mathbf{B}^\perp(\mathbf{\Phi}(\theta))[\mathbf{C}(\mathbf{\Phi}(\theta), \mathbf{\Phi}'(\theta)\dot{\theta}) + \mathbf{D}(\mathbf{\Phi}(\theta))\mathbf{\Phi}''] \tag{34}$$

$$\bar{\gamma}(\theta) = \mathbf{B}^\perp(\mathbf{\Phi}(\theta))\mathbf{G}(\mathbf{\Phi}(\theta)). \tag{35}$$

For underactuated mechanical systems under unilateral constraints, (32) should be accompanied with the reset law

$$\begin{bmatrix}\theta^+ \\ \dot{\theta}^+\end{bmatrix} = \Delta_\theta(\theta^-, \dot{\theta}^-) \tag{36}$$

where Δ_θ translates the jumps of the mechanical system (1), (2) to the jumps of the reduced dynamics (32).

The reduced system (32), (36) is referred to as the hybrid zero dynamics (Westervelt et al, 2003; Ames et al, 2012), and its solutions (if any) represent motions that, under some technical assumptions, can be imposed on the system by a proper feedback synthesis.

An appropriate periodic solution $\mathbf{q}_\star(t) = \mathbf{q}_\star(t + T_s)$ of (1)-(2) can be found by the use of a nonlinear dynamic optimization (see, e.g. the works by Aoustin and Formalsky (2003); Westervelt et al (2007)), where the motion is defined by basis functions (normally polynomials) $\mathbf{q}_\star(t)$ whose coefficients are to be specified to optimize some criteria, e.g., energy. A feasible solution

of the hybrid zero dynamics (32), (36) can thus be obtained. The resulting procedure constitutes a widely used methodology of the reference trajectory design in bipedal robotics, and it is the approach adopted in this paper. Other methods to generate periodic solutions can be found, e.g., in Arai et al (1998); Bullo and Lynch (2001); Mettin et al (2007).

Clearly, the knowledge of $\mathbf{q}_\star(t)$ allows one to construct n-scalar functions $\phi_1(\theta), \dots, \phi_n(\theta)$ that parametrize the same periodic solution $\mathbf{q}_\star(\mathbf{t})$ by the scalar variable θ. Given these VHCs, the $n+1$ quantities

$$\theta, \quad \eta_1 = q_1 - \phi_1(\theta), \dots, \eta_n = q_n - \phi_n(\theta) \tag{37}$$

can be viewed as redundant generalized coordinates for the underactuated system (1)-(2) so that one of them, can be expressed as a function of the other coordinates. Without loss of generality, η_n is assumed to be so, and the new independent coordinates are

$$\boldsymbol{\eta} = \eta_1, \dots, \eta_{n-1}{}^\top \in \mathbb{R}^{n-1} \quad \text{and} \quad \theta \in \mathbb{R} \tag{38}$$

whereas the last equality in (37) can be rewritten as

$$q_n = \phi_n(\theta) + h(\boldsymbol{\eta}, \theta) \tag{39}$$

with some smooth scalar function $h(\boldsymbol{\eta}, \theta)$. Hence, the coordinate transformation (37), (39) comes with the Jacobian matrix

$$\mathbf{L}(\theta, \boldsymbol{\eta}) = \begin{bmatrix} \mathbf{I}_{n-1} & \mathbf{0}_{(n-1)\times 1} \\ \frac{\partial h}{\partial \boldsymbol{\eta}} & \frac{\partial h}{\partial \theta} \end{bmatrix} + [\mathbf{0}_{\mathbf{n}\times(\mathbf{n-1})}, \boldsymbol{\Phi}'(\theta)]. \tag{40}$$

Provided that the Jacobian matrix is not singular in a vicinity of the desired orbit, a one-to-one relation is locally established between the first order derivatives of the new coordinates $(\boldsymbol{\eta}, \theta)^\top$ and those of the original coordinates q as

$$\dot{\mathbf{q}} = \mathbf{L}(\boldsymbol{\eta}, \theta)[\dot{\boldsymbol{\eta}}, \dot{\theta}]^\top. \tag{41}$$

Then, by substituting the relations $q_i = \eta_i - \phi_i(\theta)$, $1 \le i \le (n-1)$, $q_n = \phi_n(\theta) + h(\boldsymbol{\eta}, \theta)$, (41), (40), their derivatives $\dot{q}_i(\theta, \boldsymbol{\eta})$, $1 \le i \le (n-1)$, $\dot{q}_n(\theta, \boldsymbol{\eta})$ into (1), the state equations, governing the dynamics of $\boldsymbol{\eta}$, are obtained as follows

$$\ddot{\boldsymbol{\eta}} = \mathbf{R}(\boldsymbol{\eta}, \dot{\boldsymbol{\eta}}, \theta, \dot{\theta}) + \mathbf{N_1}(\boldsymbol{\eta}, \theta)\mathbf{w} + \mathbf{N_2}(\boldsymbol{\eta}, \theta)\boldsymbol{\Gamma}. \tag{42}$$

Moreover, one can introduce a control transformation

$$\boldsymbol{\Gamma} = \mathbf{v} + \boldsymbol{\Gamma}_\star \tag{43}$$

where $\boldsymbol{\Gamma}_\star$ is the nominal input along the nominal target trajectory $\theta = \theta_\star$, $\dot{\theta} = \dot{\theta}_\star$, $\boldsymbol{\eta} = 0$, $\dot{\boldsymbol{\eta}}$. Then, combining (42) and (43) yields the dynamics of the $\boldsymbol{\eta}$ variables in the form

$$\ddot{\boldsymbol{\eta}} = \bar{\mathbf{R}}(\boldsymbol{\eta}, \dot{\boldsymbol{\eta}}, \theta, \dot{\theta}) + \mathbf{N_1}(\theta, \boldsymbol{\eta})\mathbf{w} + \mathbf{N_2}(\theta, \boldsymbol{\eta})\mathbf{v} \tag{44}$$

where the function $\bar{\mathbf{R}} = \mathbf{R}(\boldsymbol{\eta}, \dot{\boldsymbol{\eta}}, \theta, \dot{\theta}) + \mathbf{N_2}(\theta, \boldsymbol{\eta})\boldsymbol{\Gamma}_\star$ is nullified along the desired orbit. In order to fully describe the dynamics in the new coordinates (37), it remains to incorporate the plant dynamics of θ. Following (Shiriaev et al, 2005), the local dynamics of (1) are given by

$$\begin{aligned} \bar{\alpha}(\theta)\ddot{\theta} + \bar{\beta}(\theta)\dot{\theta}^2 + \bar{\gamma}(\theta) = g_I(\boldsymbol{\eta}, \dot{\boldsymbol{\eta}}, \theta, \dot{\theta}, \ddot{\theta})I \\ + g_\eta(\boldsymbol{\eta}, \dot{\boldsymbol{\eta}}, \theta, \dot{\theta}, \ddot{\theta})\boldsymbol{\eta} + g_{\dot{\eta}}(\boldsymbol{\eta}, \dot{\boldsymbol{\eta}}, \theta, \dot{\theta}, \ddot{\theta})\dot{\boldsymbol{\eta}} + g_v(\boldsymbol{\eta}, \dot{\boldsymbol{\eta}}, \theta, \dot{\theta}, \ddot{\theta})\mathbf{v} \\ + g_w(\boldsymbol{\eta}, \dot{\boldsymbol{\eta}}, \theta, \dot{\theta}, \ddot{\theta})\mathbf{w} \end{aligned} \tag{45}$$

$$\ddot{\boldsymbol{\eta}} = \bar{\mathbf{R}}(\boldsymbol{\eta}, \dot{\boldsymbol{\eta}}, \theta, \dot{\theta}) + \mathbf{N_1}(\theta, \boldsymbol{\eta})\mathbf{w} + \mathbf{N_2}(\theta, \boldsymbol{\eta})\mathbf{v} \tag{46}$$

where the functions $g_I(\cdot)$, $g_\eta(\cdot)$, $g_{\dot{\eta}}(\cdot)$, $g_v(\cdot)$ and $g_w(\cdot)$ are smooth matrix functions of appropriate dimensions, and are nullified for $\boldsymbol{\eta} = \dot{\boldsymbol{\eta}} = \mathbf{0}$, whereas I is a solution of the differential equation

$$\dot{I} = \dot{\theta}\left[\frac{2}{\alpha(\theta)}g - \frac{2\beta(\theta)}{\alpha(\theta)}I\right] \tag{47}$$

with $g(\cdot) = g_I(\cdot)I + g_\eta(\cdot)\boldsymbol{\eta} + g_{\dot{\eta}}(\cdot)\dot{\boldsymbol{\eta}} + g_v(\cdot)\mathbf{v} + g_w(\cdot)\mathbf{w}$.

The *transversal coordinates* to the periodic motion are given by the $(2n-1)$-dimensional vector

$$\mathbf{x}_\perp = [I, \boldsymbol{\eta}, \dot{\boldsymbol{\eta}}]^\top, \tag{48}$$

which can be introduced in a vicinity of the solution

$$\eta_1 = \eta_{\star 1} = 0, \dots, \eta_{n-1} = \eta_{\star(n-1)} = 0, \quad \theta = \theta_\star. \tag{49}$$

The choice of these transverse coordinates allows one to introduce a moving Poincaré section $S(\tau)$, which is determined in a time interval $[0, T_s]$. These sections are transversal to the target trajectory at each instant of time and at each point of the motion (see (Leonov, 2006) for more details on moving Poincaré sections). In particular, the conserved quantity I, playing an important role in the transversal dynamics, is shown (Shiriaev et al, 2008) to directly relate to the Euclidean distance from the orbit, generated by the reference trajectory $\theta_\star(t)$, to the actual plant trajectory for every $t \in [0, T_s]$.

The underactuated orbital stabilization problem can now be treated, using the $\mathcal{H}_\infty$-control synthesis for fully actuated systems operating under unilateral constraints, that has been revisited in section 3.2.

4 Orbital synthesis via nonlinear $\mathcal{H}_\infty$-control

Between impacts, combining (47), (44), one arrives to the nonlinear dynamics of the transverse coordinates (48), defined by a nonlinear time-variant system of the form

$$\dot{\mathbf{x}}_\perp = \mathbf{f}(\mathbf{x}_\perp, t) + \mathbf{g_1}(\mathbf{x}_\perp, t)\mathbf{w} + \mathbf{g_2}(\mathbf{x}_\perp, t)\mathbf{v} \tag{50}$$

To complete this model, one needs to complement (50) with its corresponding impact map. This can be done by applying the instantaneous transformation proposed in (Freidovich et al, 2008), that allows to introduce the impact law as

$$\mathbf{x}_{\perp}^{+} = \mathcal{F}\mathbf{x}_{\perp}^{-} + \mathbf{w}_{\perp}^{\mathbf{d}} \tag{51}$$

with

$$\mathcal{F} = \mathbf{P}^{+}_{\mathbf{n(0)}} \mathrm{d}\bar{\mathbf{F}} \mathbf{P}^{-}_{\mathbf{n(T_s)}} \tag{52}$$

$$\mathbf{P}^{+}_{\mathbf{n(0)}} = \mathbf{L_c}(0)\left(\mathbf{I} - \frac{\mathbf{n}(0)\mathbf{n}^{\top}(0)}{\mathbf{n}^{\top}(0)\mathbf{n}(0)}\right) \tag{53}$$

$$\mathbf{P}^{-}_{\mathbf{n(T_s)}} = \left(\mathbf{I} - \frac{\mathbf{n}(T_s)\mathbf{m}^{\top}(T_s)}{\mathbf{n}^{\top}(T_s)\mathbf{m}}\right)\begin{bmatrix}\mathbf{L_c}(T_s)\\ \mathbf{n}^{\top}(T_s)\end{bmatrix}^{-1}\begin{bmatrix}\mathbf{I}\\ \mathbf{0}\end{bmatrix} \tag{54}$$

where $\bar{\mathbf{F}}$ is the map from the pre-impact states $(\mathbf{q}^{-}, \dot{\mathbf{q}}^{-})$ to the post-impact states $(\mathbf{q}^{+}, \dot{\mathbf{q}}^{+})$, T_s is the period of the target trajectory, $\mathbf{I}$ is an identity matrix of the appropriate dimensions (not to be confused with the scalar I, which is the solution of (47)), $w_{\perp}^{d}$ accounts for inaccuracies in the restitution law, $\mathbf{m}$ is a normal vector to the linearization of the switching surface, $\mathbf{n}(t) = [\dot{\mathbf{q}}_{\star}^{\top}(t), \ddot{\mathbf{q}}_{\star}(t)]^{\top}$ and $\mathbf{L_c}(\cdot)$ defines the Jacobian matrix of the coordinate transformation

$$[\Delta I, \Delta\boldsymbol{\eta}^{\top}, \Delta\dot{\boldsymbol{\eta}}^{\top}]^{\top} = \mathbf{L_c}(t)[\Delta\mathbf{q}^{\top}, \Delta\dot{\mathbf{q}}^{\top}]^{\top} \tag{55}$$

that relates the linear parts of the increments of the transverse coordinates and the linear parts of increments of the generalized coordinates, which in turn can be computed from the relations (37) and the formulas

$$\left.\frac{\partial I}{\partial\theta}\right|_{\substack{\theta=\theta_{\star}(t)\\ \dot{\theta}=\dot{\theta}_{\star}(t)}} = -2\ddot{\theta}_{\star}(t), \quad \left.\frac{\partial I}{\partial\dot{\theta}}\right|_{\substack{\theta=\theta_{\star}(t)\\ \dot{\theta}=\dot{\theta}_{\star}(t)}} = 2\dot{\theta}_{\star}(t). \tag{56}$$

For more details on this formulation, see the works by Freidovich et al (2008); Freidovich and Shiriaev (2009).

Clearly, (50)-(51) define a hybrid linear system that can be stabilized using the nonlinear $\mathcal{H}_{\infty}$ control theory presented before. The following result is in order.

Theorem 3 *Consider the nonlinear time-variant hybrid system* (50)-(51)*. Let conditions C1), C3) and* (19) *be satisfied with some* $\gamma > 0$*. Then the transverse system* (50)-(51) *driven by the state feedback*

$$\mathbf{v} = -\mathbf{g_2}^{\top}\mathbf{P}_{\varepsilon}(s(\theta))\mathbf{x}_{\perp} \tag{57}$$

locally possesses a $\mathcal{L}_2$*-gain less than* γ*, where* $s(\theta)$ *is an index parametrizing the particular leaf of the moving Poincaré section, to which the vector* $x_{\perp}$ *belongs at time moments* t*, i.e. a smooth function that satisfies the identity* $s(\theta_{\star}) = t$ *for all* $t \in [0, T_s]$*. Moreover, the disturbance-free closed-loop transverse system* (5)-(7), (57) *is uniformly asymptotically stable, which renders the desired orbit* (3) *orbitally asymptotically stable.*

Proof The proof can be obtained by applying theorem 2 to the nonlinear hybrid system (50)-(51).

The solution $\mathbf{P}_{\varepsilon}(t)$ of the differential Riccati equation (16), subject to the boundary condition (23), relies on the transverse linearization (15) of the nonlinear dynamics (50) along the desired motion (49), after an output to be controlled (13) has been defined.

This result will be used in the next section to orbitally stabilize a five-link underactuated biped.

5 Case study: $\mathcal{H}_{\infty}$-Control Synthesis for of an Underactuated Planar Five-Link Bipedal Robot

The objective of this section is to extend the results of the previous section to the robust orbital stabilization of an underactuated bipedal robot using position feedback.

5.1 Model of a Planar Five-Link Bipedal Robot

The bipedal robot considered in this section is walking on a rigid and horizontal surface. It is modeled as a planar biped, which consists of a torso, hips, two legs with knees but no actuated ankles (see Fig. 2). The walking gait is composed of single support phases and impacts. The complete model of the biped robot consists of two parts: the differential equations describing the dynamics of the robot during the swing phase, and an impulse model of the contact event (the impact between the swing leg and the ground is modeled as a contact between two rigid bodies as in the work of Chevallereau et al (2003)). It is assumed that the only measurements available are the joints positions, since no velocity sensors are used. During the single-support phase, the degree of underactuation equals one. Let us assume the stance leg tip is acting as a pivot on the ground, *i.e.*, there is no slipping and no take off of the stance leg tip. Then the biped's model in single support phase between successive impacts can be written:

$$\begin{pmatrix} D_{11} & \mathbf{D_{12}}\\ \mathbf{D_{21}} & \mathbf{D_{22}}\end{pmatrix}\begin{pmatrix}\ddot{q}_1\\ \ddot{\mathbf{q}}_{\mathbf{a}}\end{pmatrix} + \begin{pmatrix} H_1\\ \mathbf{H_2}\end{pmatrix} = \begin{pmatrix}0\\ \boldsymbol{\Gamma}\end{pmatrix} + \begin{pmatrix} w_1\\ \mathbf{w_2}\end{pmatrix} \tag{58}$$

where $\mathbf{q} = (q_1, q_2, q_3, q_4, q_5)^{\top}$ the 5×1 vector of generalized coordinates, $\mathbf{q_a} = (q_2, q_3, q_4, q_5)^{\top}$ the 4×1 vector of actuated joint angles, $\boldsymbol{\Gamma} = (\Gamma_1, \Gamma_2, \Gamma_3, \Gamma_4)^{\top}$ is the 4×1

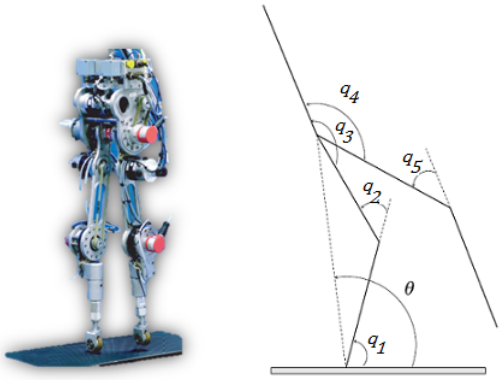

Fig. 2 Left: Five-link bipedal planar robot Rabbit (Chevallereau et al, 2003). Right: 2D Representation, joint positions (q_i) placement and geometrical interpretation of the virtual leg angle θ.

vector of joint torques (see Fig. 2), $\mathbf{H} = \mathbf{C}(\mathbf{q}, \dot{\mathbf{q}})\dot{\mathbf{q}} + \mathbf{G}(\mathbf{q})$ $= [H_1, \mathbf{H_2}^\top]^\top$ and $\mathbf{w_c}$ is the 5×1 vector of disturbances, with components w_1 and $\mathbf{w_2}$ representing the disturbances in the underactuated and actuated subsystems, respectively. D_{11} and H_1 are scalars, $\mathbf{D_{12}}$ is a 1×4 vector, $\mathbf{D_{21}}$ and $\mathbf{H_2}$ are 4×1 vectors and $\mathbf{D_{22}}$ is a 4×4 matrix.

The double support phase is instantaneous, so an impact appears when the swing leg tip touches the ground, at an *a priori* unknown collision time instant $t = T_I$; for this time the swing leg touches the ground. It is assumed that the impact is passive, absolutely inelastic, and that the legs do not slip. The corresponding algebraic equations for the velocities jumps, *i.e.* the restitution law (2), can be obtained through integration of biped's equations of motions, taking into account the ground reactions, for the infinitesimal time from T_I^- to T_I^+. Its analytic expression can be found in (Djoudi et al, 2005).

Model (1) was written taking into account implicitly the contact between the stance leg and the ground, without take-off nor sliding. Since just after the impact, the legs exchange their role, the former swing leg must now become the stance leg and vice versa, a change of coordinates after the impact is necessary. This coordinate swap is included as part of the impact map (Chevallereau et al, 2003). The overall bipedal robot model can be expressed as a nonlinear system with impulse effects (5), where $F(q)$ being the altitude of the swing leg tip, and $\mathbf{w_d}$ accounts for external disturbances in the impact phase, such as modelling errors, uneven ground, etc.

5.2 Motion Planning

The control of the biped for the walking gait, consists in tracking a reference trajectory $(\mathbf{q}_\star(\theta)^\top, \dot{\mathbf{q}}_\star(\theta, \dot{\theta})^\top)^\top$. The under-actuation characteristic of the biped in single support phase has to be taken into account because it is not possible to prescribe the five generalized coordinates independently of the biped's dynamic with only four torques. An instantaneous double support phase is considered. The trajectory is then obtained using a nonlinear dynamics optimization (Chevallereau et al, 2003; Miossec and Aoustin, 2006; Tlalolini et al, 2011)

The well known approach of virtual constraints (Grizzle et al, 2001; Aoustin and Formalsky, 2003; Westervelt et al, 2007) was used for the definition of the motion. These virtual constraints are imposed as reference trajectories over the actuated coordinates $\mathbf{q_a}$, and they are chosen to be functions of the geometric variable

$$\theta = q_1 + 0.5q_2 \tag{59}$$

instead of time (Aoustin et al, 2006). This variable θ represents the angle of the line connecting the stance leg end to the hip against the floor, and is strictly monotonic along each step. These functions are chosen as Bézier polynomials of fifth order (Bezier, 1972). The specific choice of the Bézier polynomial coefficients is accomplished on the basis of achieving invariance of the biped's hybrid zero dynamics (32), (36), and the minimization of a sthenic criterion (minimization of the motors energy) in order to reduce the torques peak demands over a step. The solution of this optimization problem also takes into account a set of nonlinear constraints that ensures that there is no take off of the support leg end, that the support leg end does not slide on the floor, and that the swing leg end height ensures that a contact with the ground will appear only at the end of the step. For more details, the interested reader can consult the work by Westervelt et al (2004).

5.3 $\mathcal{H}_\infty$ Control synthesis

The objective of this section is to apply the results of section IV to orbitally stabilize the underactuated bipedal robot to the desired motion presented in the previous section, supposing that both positions and velocities are measured. Afterwards, assuming that only positions are available for measurements, $\mathcal{H}_\infty$ output feedback synthesis is involved to estimate the missing velocities.

5.3.1 State Feedback Synthesis

The control objective for the 5-link bipedal robot is to design a nonlinear $\mathcal{H}_\infty$ position feedback controller that follows a pre-specified periodic motion

$$\mathbf{q}_\star(\theta) = \mathbf{\Phi}(\theta) = [\phi_1(\theta), \phi_2(\theta), \phi_3(\theta), \phi_4(\theta), \phi_5(\theta)]^\top \quad (60)$$

$$\dot{\mathbf{q}}_\star(\theta, \dot{\theta}) = \mathbf{\Phi}'(\theta) = \frac{\partial \mathbf{\Phi}(\theta)}{\partial \theta}\dot{\theta} \quad (61)$$

$$\ddot{\mathbf{q}}_\star(\theta, \dot{\theta}, \ddot{\theta}) = \mathbf{\Phi}''(\theta) = \frac{\partial \mathbf{\Phi}(\theta)}{\partial \theta}\dot{\theta}^2 + \frac{\partial^2 \mathbf{\Phi}(\theta)}{\partial \theta^2}\ddot{\theta} \quad (62)$$

Let us define the error variables

$$\eta_1 = q_2 - \phi_2(\theta), \dots \; \eta_4 = q_5 - \phi_5(\theta) \quad (63)$$

and the error vector $\boldsymbol{\eta} = [\eta_1, \dots, \eta_4]^\top$. Introducing the control transformation

$$\mathbf{\Gamma} = \left(\mathbf{H_2} - \frac{\mathbf{D_{21}}}{D_{11}}H_1\right) + \mathbf{D_T}(\mathbf{\Phi}''_{\mathbf{a}}(\theta) + \mathbf{v}), \quad (64)$$

specified with $\mathbf{D_T} = \mathbf{D_{22}} - \frac{\mathbf{D_{21}D_{12}}}{D_{11}}$ and $\mathbf{\Phi}''_{\mathbf{a}}(\theta) = [\phi''_2(\theta), \dots, \phi''_5(\theta)]^\top$, the dynamics (44) can be represented in the form of the disturbed double integrator

$$\ddot{\boldsymbol{\eta}} = \mathbf{v} + \mathbf{D_T^{-1}}\mathbf{w_2}, \quad (65)$$

where $\mathbf{w_2}$ is the disturbance, affecting the actuated subsystem of (58).

By left-multiplying (58) by the ortogonal matrix $\mathbf{B}^\perp(\mathbf{q}) = [1, 0, 0, 0, 0]$, and combining it with (62), one can obtain the dynamics (32), (36) as follows

$$\ddot{\theta} = \frac{-\left(\frac{D_{11}}{2}\frac{\partial^2 \phi_2(\theta)}{\partial \theta^2} + \mathbf{D_{12}}\frac{\partial^2 \mathbf{\Phi_a}(\theta)}{\partial \theta^2}\right)\dot{\theta}^2 - H_1}{D_{11}\left(1 - \frac{1}{2}\frac{\partial \phi_2(\theta)}{\partial \theta}\right) + \mathbf{D_{12}}\frac{\partial \mathbf{\Phi_a}(\theta)}{\partial \theta}} \quad (66)$$

$$\begin{bmatrix}\theta^+ \\ \dot{\theta}^+\end{bmatrix} = \Delta_\theta(\theta^-, \dot{\theta}^-) = \theta \circ \mu(\mathbf{q}_\star(\theta)^-, \dot{\mathbf{q}}_\star(\theta)^-) \quad (67)$$

with $\mathbf{\Phi_a}(\theta) = [\phi_2(\theta), \dots, \phi_5(\theta)]^\top$. ¿From (66), one can clearly identify the terms $\bar{\alpha}(\theta)$, $\bar{\beta}(\theta)$ and $\bar{\gamma}(\theta)$. The denominator term of (66), which corresponds to $\bar{\alpha}(\theta)$ in (32), is a virtual inertia of the biped with respect to the contact point between the leg tip and the ground (Chevallereau et al, 2003). This virtual inertia term can cross zero during a walking gait. However the optimization algorithm of getting the reference trajectory $\mathbf{q_{a\star}}(\theta)$ involves a constraint that ensures this term to be non-zero.

Therefore, by using the transverse coordinates $\mathbf{x}_\perp = [I.\boldsymbol{\eta}^\top, \dot{\boldsymbol{\eta}}^\top]^\top$, one can rewrite the biped dynamics in the form (50), (51), being specified with

$$\mathbf{f}(\mathbf{x}_\perp, t) = \begin{bmatrix} -\frac{2\dot{\theta}\bar{\beta}(\theta)}{\bar{\alpha}(\theta)}I \\ \dot{\boldsymbol{\eta}} \\ \mathbf{0} \end{bmatrix}, \quad (68)$$

$$\mathbf{g_1}(\mathbf{x}_\perp, t) = \begin{bmatrix} \frac{2\dot{\theta}}{\bar{\alpha}(\theta)} & \mathbf{0_{1\times 4}} \\ \mathbf{0_{4\times 1}} & \mathbf{0_{4\times 4}} \\ \mathbf{0_{4\times 1}} & \mathbf{D_T^{-1}} \end{bmatrix}, \quad (69)$$

$$\mathbf{g_2}(\mathbf{x}_\perp, t) = \begin{bmatrix} \frac{2\dot{\theta}}{\bar{\alpha}(\theta)}(D_{11}\mathbf{K}_\perp - \mathbf{D_{12}}) \\ \mathbf{0_{4\times 4}} \\ \mathbf{I_{4\times 4}} \end{bmatrix}, \quad (70)$$

$$\mathbf{K}_\perp = \left[\frac{1}{2}, 0, 0, 0\right], \quad (71)$$

$$\mathcal{F} = \mathbf{P}^+_{\mathbf{n(0)}}\mathrm{d}\mu(\mathbf{q}, \dot{\mathbf{q}})\mathbf{P}^-_{\mathbf{n(T_s)}} \quad (72)$$

with θ, $\dot{\theta}$ taken along the predefined solution of (66), and the matrices $\mathbf{P}^+_{\mathbf{n(0)}}$, $\mathbf{P}^-_{\mathbf{n(T_s)}}$ come from the instant transformation (52)-(54) applied to the restitution function $\mu(\mathbf{q}^-, \dot{\mathbf{q}}^-)$ (Freidovich et al, 2008). The matrices $\mathbf{0_{n\times m}}$ and $\mathbf{I_{n\times m}}$ represent zero and identity matrices of dimensions $n \times m$.

It remains to define the output to be controlled (6). Inspired by the work of Isidori and Astolfi (1992), such an output can be written as

$$\mathbf{z} = \begin{bmatrix}\mathbf{0_{1\times 4}} & \rho_0 I & \rho_1 \boldsymbol{\eta}^\top & \rho_2 \dot{\boldsymbol{\eta}}^\top\end{bmatrix}^\top + \mathbf{v}^\top \begin{bmatrix}\mathbf{I_{4\times 4}} & \mathbf{0}^\top_{\mathbf{9\times 4}}\end{bmatrix}^\top \quad (73)$$

which satisfies (9), with ρ_0, ρ_1, ρ_2 being positive scalars. Finally, the controller $\mathbf{v}$ can be synthesized by applying theorem 3 to the transverse system (50), (51) specified with (68)-(72), considering the output (73).

Since the feedback transformation (64) and the $\mathcal{H}_\infty$ controller (57) make use of the measurements of positions and velocities, in the next section, the output feedback synthesis is developed in order to estimate the non-measured velocities.

5.3.2 Output feedback synthesis

According to (1)-(2), the desired periodic motion corresponding to the orbit $\mathcal{O}_\star$ is governed by

$$\mathbf{D}(\mathbf{q}_\star)\ddot{\mathbf{q}}_\star + \mathbf{H}(\mathbf{q}_\star, \dot{\mathbf{q}}_\star) = \mathbf{B}\mathbf{\Gamma}^{\mathbf{s}}_\star. \quad (74)$$

The input torque $\mathbf{\Gamma}^{\mathbf{s}}_\star$ is designed as (64), which forces the dynamics of (1), (2), (43), (57) to stay on the periodic orbit $\mathcal{O}_\star$ when the system is started on $\mathcal{O}_\star$. Since $\mathbf{\Gamma}^{\mathbf{s}}_\star$ relies on the measurement of the generalized positions and velocities (the latter not available), $\mathbf{\Gamma}$ is substituted by the dynamic controller

$$\mathbf{\Gamma} = \mathbf{\Gamma}^{\mathbf{s}}_\star + \mathbf{u}(\boldsymbol{\xi}, t) \quad (75)$$

where $\mathbf{u}(\boldsymbol{\xi},t)$ has the form (10), and its internal state $\boldsymbol{\xi}$ provides an estimation of the non-measured variables. This can be done by defining the state vectors $\mathbf{x_1}=\mathbf{q}-\mathbf{q}_\star$, $\mathbf{x_2}=\dot{\mathbf{q}}-\dot{\mathbf{q}}_\star$, and combining (1), (4) and (74), the error dynamics can be rewritten as

$$\begin{aligned}\dot{\mathbf{x}}_\mathbf{1} &= \mathbf{x_2}\\ \dot{\mathbf{x}}_\mathbf{2} &= \mathbf{D}(\mathbf{x_1}+\mathbf{q}_\star)^{-\mathbf{1}}[\mathbf{D}(\mathbf{q}_\star)\ddot{\mathbf{q}}_\star+\mathbf{H}(\mathbf{q}_\star,\dot{\mathbf{q}}_\star)\\ &\quad -\mathbf{H}(\mathbf{x_1}+\mathbf{q}_\star,\mathbf{x_2}+\dot{\mathbf{q}}_\star)+\mathbf{Bu}+\mathbf{w_c}]-\ddot{\mathbf{q}}_\star\end{aligned} \tag{76}$$

with an output to be controlled (6) inspired by the work of Isidori and Astolfi (1992), which satisfies (9) and can be written as

$$\mathbf{z}=\rho_3\left[\mathbf{0_{1\times 4}}\ x_{1_2}\ x_{1_3}\ x_{1_4}\ x_{1_5}\right]^\top+\mathbf{u}^\top\left[\mathbf{I_{4\times 4}}\ \mathbf{0_{4\times 4}}\right]^\top \tag{77}$$

where $x_{1_i}=q_i-q_{i\star}$, $i=2,3,4,5$ (so only the actuated coordinates error $\mathbf{q_a}-\mathbf{q_{a\star}}$ is considered), ρ_3 is a positive scalar, and with the set of measurements

$$\mathbf{y}=\mathbf{x_1}+\mathbf{w_y} \tag{78}$$

where $\mathbf{w_y}$ is a 5×1 vector of measurement disturbances (for a practical application, in order to estimate the absolute orientation, and thus q_1 and θ, the use of an inertial measurement unit is introduced section 5.4.2). Thus, the generic system (5)-(7) can be specified with

$$\begin{aligned}\mathbf{f}(\mathbf{x},t)&=\begin{bmatrix}\mathbf{x}_2\\ \mathbf{D}(\mathbf{x_1}+\mathbf{q}_\star)^{-\mathbf{1}}[\mathbf{H}(\mathbf{q}_\star,\dot{\mathbf{q}}_\star)+\mathbf{D}(\mathbf{q}_\star)\ddot{\mathbf{q}}_\star]\end{bmatrix}\\ &+\begin{bmatrix}\mathbf{0_{5\times 1}}\\ -\mathbf{D}(\mathbf{x_1}+\mathbf{q}_\star)^{-\mathbf{1}}[\mathbf{H}(\mathbf{x_1}+\mathbf{q}_\star,\mathbf{x_2}+\dot{\mathbf{q}}_\star)]-\ddot{\mathbf{q}}_\star\end{bmatrix}\end{aligned} \tag{79}$$

$$\mathbf{g_1}(\mathbf{x},t)=\begin{bmatrix}\mathbf{0_{5\times 5}} & \mathbf{0_{5\times 5}}\\ \mathbf{0_{5\times 5}} & \mathbf{D}(\mathbf{x_1}+\mathbf{q}_\star)^{-\mathbf{1}}\end{bmatrix}, \tag{80}$$

$$\mathbf{g_2}(\mathbf{x},t)=\begin{bmatrix}\mathbf{0_{5\times 4}}\\ \mathbf{D}(\mathbf{x_1}+\mathbf{q}_\star)^{-\mathbf{1}}\mathbf{B}\end{bmatrix},\ \mathbf{h_1}(\mathbf{x})=\begin{bmatrix}\mathbf{0_{4\times 1}}\\ \rho_1\mathbf{K_o}\mathbf{x}_1\end{bmatrix}, \tag{81}$$

$$\mathbf{k_{12}}(\mathbf{x})=\begin{bmatrix}\mathbf{I_{4\times 4}}\\ \mathbf{0_{4\times 4}}\end{bmatrix},\ \mathbf{K_o}=\left[\mathbf{0_{4\times 1}}\ \mathbf{I_{4\times 4}}\right], \tag{82}$$

$$\mathbf{h_2}(\mathbf{x})=\mathbf{x_1},\ \mathbf{k_{21}}(\mathbf{x})=\left[\mathbf{I_{5\times 5}}\ \mathbf{0_{5\times 5}}\right], \tag{83}$$

$$\boldsymbol{\Delta}(\mathbf{x},t)=\mu(\mathbf{x_1}+\mathbf{q}_\star,\mathbf{x_2}+\dot{\mathbf{q}}_\star)-\mu(\mathbf{q}_\star,\dot{\mathbf{q}}_\star), \tag{84}$$

$$F(\mathbf{x},t)=F_0(\mathbf{x_1}+\mathbf{q}_\star),\quad \boldsymbol{\omega}(\mathbf{x},t)=\mathbf{I_{5\times 5}} \tag{85}$$

where the function $F_0(\mathbf{q})$ is given by the swing foot height.

If the output (6) specified with (82) is driven to zero, the system will be driven to the zero dynamics manifold

$$\mathcal{Z}=\{(\mathbf{q},\dot{\mathbf{q}})|\mathbf{q_a}=\mathbf{q_{a\star}}(\theta),\dot{\mathbf{q}}_\mathbf{a}=\frac{\partial\mathbf{q_{a\star}}(\theta)}{\partial\theta}\dot{\theta}\} \tag{86}$$

and the dynamic behavior of θ (restriction dynamics) will be given by the hybrid zero dynamics (66), (67).

Finally, the last theorem of this work is presented below.

Theorem 4 *Let conditions C1)-C4) be satisfied for the hybrid system* (5)-(8) *specified with* (79)-(85). *Then, the dynamic control* (21)-(22) *is a solution to the* $\mathcal{H}_\infty$*-control problem for the closed-loop mechanical system* (1)-(2), (75).

Proof The rigorous proof, following the Hamilton-Jacobi-Isaacs approach applied in the transversal coordinates, is rather technical and too lengthy to present it within the scope of the present paper. Instead, in section 6 we present numerical evidences by computing the corresponding Poincare map.

This method has been successfully implemented to orbitally stabilize periodic orbits in unrestricted mechanical systems of underactuation degree 1 (see Meza-Sanchez et al (2011)).

Thus, in the disturbed case, even if the output (6), (77) is not driven to zero, the $\mathcal{L}_2$-gain (11) of the system is still locally less than the specified value γ, keeping the output bounded around zero.

It is important to remark that $\dot{\theta}$ and $\ddot{\theta}$, necessaries to define the desired velocities $\dot{\mathbf{q}}_\star$ and accelerations $\ddot{\mathbf{q}}_\star$, need to be estimated, since only position measurements are considered; this estimation is effectuated using the states from (21).

This result will be used in the next section to robustly stabilize a planar and underactuated biped robot on a desired periodic orbit.

5.4 Numerical tests

The parameters considered in this section are those of "Rabbit" (Chevallereau et al, 2003). Here the application of the control law (75) is considered to track a geometrical-reference trajectory defined using a virtual constraints approach. The period and the length of the nominal walking gait, which is obtained by optimization, are 0.56 s and 0.45 m. The average walking velocity is 0.80 $m\cdot s^{-1}$. This cyclic walking gait was tested in closed loop for several steps.

The control synthesis is performed in two steps. The first step consists in designing the state feedback control (57), (64) via the application of Theorem 3 to the transverse dynamics (50), (51), specified with (68)-(72). The matrices $\mathbf{A}$, $\mathbf{B_1}$, $\mathbf{B_2}$ and $\mathbf{C_1}$ used in (16) come from the transverse linearization (12), (13) of this transversal system. By iterating on γ and ε, a minimal value γ_{min} is to be found among all γ such that on the period T_s, (16) possesses a positive definite solution $\mathbf{P}_\varepsilon(t)$ for some $\varepsilon>0$ provided that relation (23)) holds true for the solution values at the initial time instant t_0 and at the first impact time instant

$t_1 = t_0 + T_s$. Then, this solution should be continued to the right with the periodicity T_s. Since generally speaking, $\mathbf{P}_\varepsilon(t_0) \neq \mathbf{P}_\varepsilon(t_1)$, the resulting T_s-periodic function $\mathbf{P}_\varepsilon(t)$ is expected to undergo discontinuities at the impact time instants $t_i = t_0 + iT_s$, $i = 1, 2, \ldots$. Specifying the values $\rho_0 = 1$, $\rho_1 = 200$, $\rho_2 = 10$ and following the above iteration procedure, a value $\gamma_{min} \approx 8000$ is found for $\varepsilon = 0.001$. To avoid dealing with high controller gains, the value $\gamma = 10000$ is subsequently used in the simulation runs.

Figure 3 illustrates the eigenvalues of the periodic solution $\mathbf{P}_\varepsilon(t)$, thus obtained. It is observed from the figure that the periodic eigenvalues, also undergoing discontinuities at the impact time instants, remain positive definite along the period. The positive definiteness of $\mathbf{P}_\varepsilon(t)$ is thus confirmed for all $t \geq 0$.

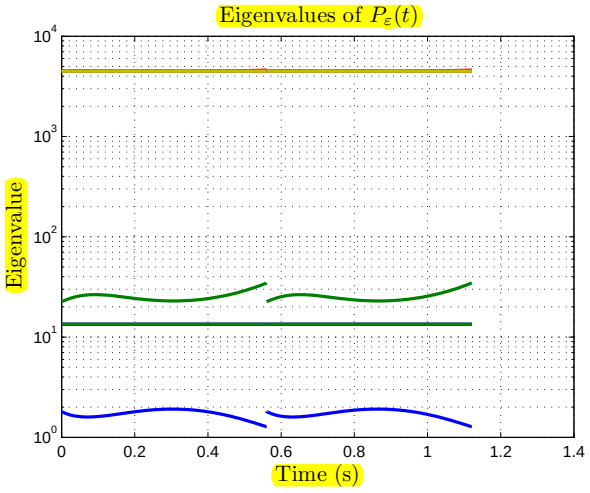

Fig. 3 The eigenvalues of the solution $\mathbf{P}_\varepsilon(t)$ of (16), plotted for two steps. Due to the multiplicity of the eigenvalues, only four distinct eigenvalues among nine are plotted.

The second step consists of the design of the output feedback synthesis (75), where $\mathbf{\Gamma}^{\mathbf{s}}_\star$ is the state feedback control (64) designed in the previous step, and $\mathbf{u}(\boldsymbol{\xi}, t)$ is calculated applying Theorem (4) to the hybrid system (5)-(8) specified with (79)-(85). The controller parameters to be used in (16) and (17) are chosen to enforce C1)- C4) through setting a positive value for ρ_3 and γ is set to the value found in the previous step. Also, it is important to consider that a higher value of ρ_3 provides faster stabilization (which is important in order to reach the smallest possible vicinity of the reference trajectory, fast enough before the next impact appears), but as it increases it also leads to increase the controller gain of $\mathbf{u}$. Variable ε in (16)-(17) is set to once again set to a small value, only to guarantee asymptotical stability. Using the value $\rho_3 = 100$, and setting $\varepsilon = 0.001$, and $\gamma = 10000$, (16)-(17) are verified to have a symmetric positive definite and periodic solution, and $\mathbf{u}$ is calculated from (21)-(22). The non-measured velocities needed for step 1, are estimated using (21).

For every case in the following subsections, the reaction forces were verified in order to ensure that the legs do not slip nor take off.

5.4.1 Undisturbed case

Figure 4 presents the phase plane $\theta, \dot{\theta}$ for the undisturbed plant dynamics (1)-(2) ($\mathbf{w_0} = \mathbf{w_c} = \mathbf{w_d} = \mathbf{0}$), where the initial conditions of the plant (positions and velocities) were deviated 5% from the reference motion initial condition (the estimator (21) initial conditions were the reference motion initial condition, so an initial estimation error also exists). It can be seen that the plant evolution converges asymptotically to a limit cycle (depicted in blue), which represents the reference motion limit cycle. This asymptotical convergence can also be appreciated from the Poincaré map presented in Fig. 5, where a Poincaré section is taken at $\theta = \pi/2\ rad$ (black line in Fig. 4), where it is clear that the plant dynamics evolves towards a fixed point, given by the blue line. It is important to remark that this Poincaré section is chosen instead of the predefined impact configuration ($\theta = \theta_f$), since in the disturbed scenario this configuration may be different due to the influence of the external disturbances.

When the dynamics of variable θ converge to the limit cycle, all of the joints positions will converge as well, as can be seen from Fig. 6 for the first four steps; after a short transitory response (evident during the first step, i.e. between $t = 0$ and $t = 0.55\ s$), all the joints attain a periodic behavior. This fact will be taken into account to present the results of the following sections.

5.4.2 Noise in orientation measurement

In the case of the measurement of q_1, which is needed for developing the present algorithm, the biped Rabbit is not equipped with a sensor that measures this coordinate accurately (Chevallereau et al, 2003). An alternative way to estimate q_1 would be from the measurement of orientation from an inertial measurement unit (IMU). IMUs are very useful sensors that can report measurements about three axes, reducing the number of independent sensors needed on the robot. However, the use of an IMU may present some problems rising from nonlinearities or systematic error in the sensor as well as random sensor noise (Angelosanto, 2008). Whereas the Kalman filter has been used to reduce the effect of

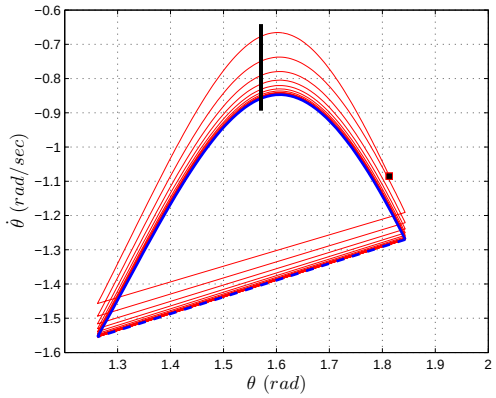

Fig. 4 Phase plane of θ for the undisturbed plant dynamics, with non-zero initial conditions, for 18 steps. Red: Plant evolution converging to a limit cycle. Blue: Reference motion limit cycle. The initial point is indicated by the black square.

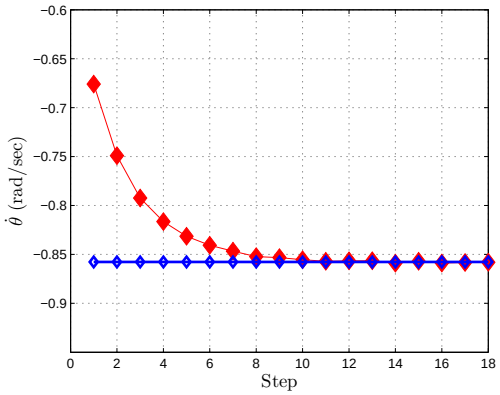

Fig. 5 Poincaré Mapping at $\theta = \pi/2\ rad$, of the undisturbed plant dynamics, with non-zero initial tracking errors, for 18 steps. Red: Plant evolution converging to a fixed point. Blue: Reference motion fixed point.

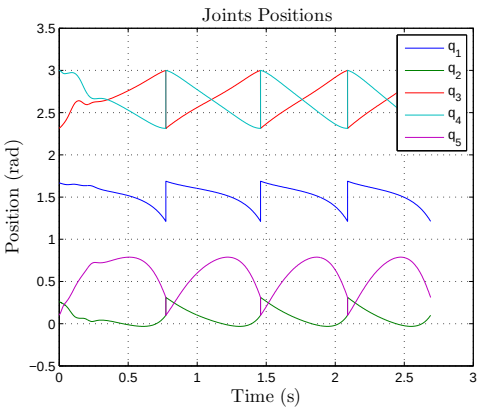

Fig. 6 Joint positions for the undisturbed system, with non-zero initial conditions. After a transitory evolution, evident during the first step, all the joints converge to a periodic motion.

the noise in the measurements in many robotic applications (see for example the work from Alcaraz-Jiménez et al (2013)), in this work the estimator (21), included in the synthesis presented in theorem 1, was used.

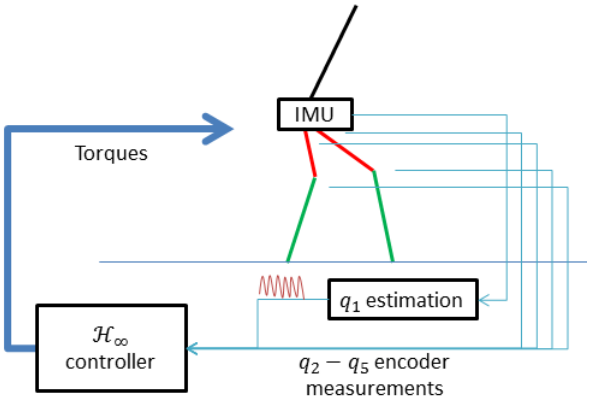

Fig. 7 IMU connection to the $\mathcal{H}_\infty$-controller.

By simulating an IMU similar to the presented at Alcaraz-Jiménez et al (2013), with 1% precision in the range of $\pm 2G$ accelerations, the controller was tested (see Fig. 7) considering that the plant is started at the same initial conditions as the reference motion (so the effects of the disturbances introduced by the IMU are separately analyzed). The IMU is considered to be placed at the hip (as shown in Fig. 7); when the biped is in simple support, by considering the measurements of the horizontal and vertical accelerations, a_x and a_y, passing both by a double integrator, the unmeasurable coordinate q_1 (and in consequence, θ) is estimated using the knowledge of the geometrical relations (see Fig. 2) between the position of the IMU (hip), the lengths of the legs and the measurable angle q_2; then white noise was introduced in order to attain the desired precision. The dynamics of θ after several steps, achieve the cycle shown in Fig. 8. It can be seen that a stable cycle, around the nominal cycle, is attained even after 8 steps.

Then, it was tested again, considering a 10% of error in the measurement considering again white noise. The behavior of the estimator (21) is shown in Fig. 9, where it can clearly be seen the attenuation effect of the $\mathcal{H}_\infty$-estimator. The resulting Poincaré map after 8 steps of this disturbed system is shown in Fig. 10, where a maximum deviation of 0.23 rad/sec is obtained and stable walking is achieved.

5.4.3 Floor height variation

As it was done in the work by Dai and Tedrake (2013), an analysis of the biped walking over uneven terrain is made (see Fig. 11). In the former article, the virtual

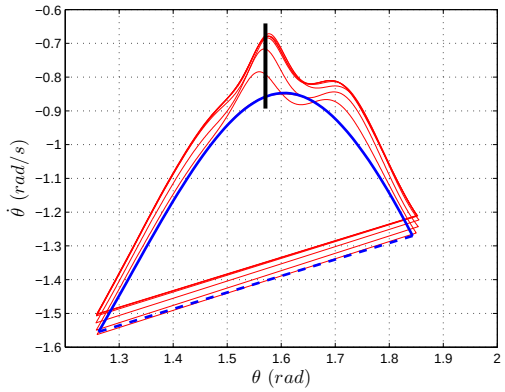

Fig. 8 Phase plane of θ, $\dot{\theta}$, for the behavior obtained by estimating q_1 from an IMU with 1% precision, under the presence of white noise, for 8 steps. Blue: nominal cycle. Red: actual cycle.

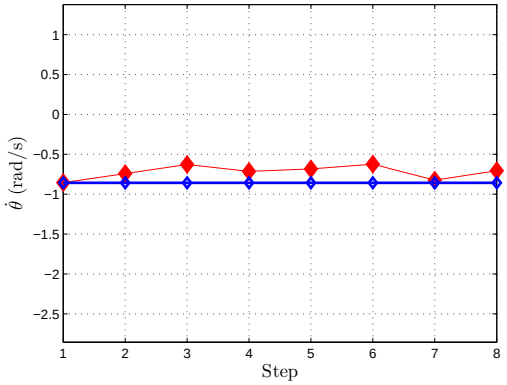

Fig. 10 Poincaré Map for the system with noise measurements, for 8 steps, with 10% error in q_1. Blue: nominal cycle. Red: actual cycle.

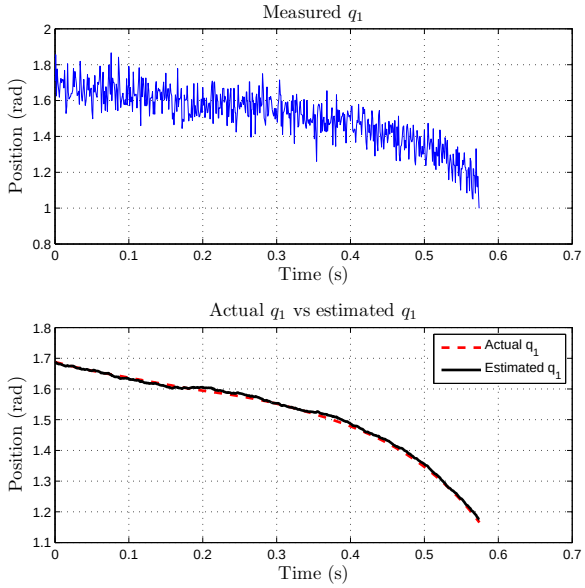

Fig. 9 Estimation of q_1 using the $\mathcal{H}_\infty$-estimator (21), along one step.

slope for the same biped robot was varied from $-2°$ to $2°$. Also, a perfect knowledge of the generalized positions and velocities was assumed. A direct comparison cannot be made for two reasons: first, the introduction of the estimator (21) increases the minimum value of γ that can be achieved (in Dai and Tedrake (2013), a $\gamma \in [5000, 6000]$ is used, whereas in the present work a minimum value of $\gamma_{min} = 9800$ is obtained using the iterative process described at the beginning of section 4). The second is that in (Dai and Tedrake, 2013), the authors do not use reference trajectories based on the virtual constraint approach, but rather trajectories defined as functions of time. It has been demonstrated that if trajectories defined as a function of time are compared against trajectories defined using the virtual constraints approach, the latter exhibits better disturbance attenuation than the former, even without the use of a robust controller (Montano et al, 2015b). Therefore, in this work, the combination of virtual constraints with the robust control synthesis, allows one to vary the slope up to $10°$, and stable walking is still achieved. The results are shown in Fig. 12 for three different cases: disturbance of the first step with a virtual slope of $5°$ (red); disturbance at the first two steps with virtual slopes of $-2°$ and $10°$ respectively (black); and alternating virtual slopes of $-5°$ and $5°$ (magenta). Again, as predicted by the theory, when the disturbances dissapear (black and red cases), the system returns to the reference cycle (blue line), whereas if the disturbance is sustained (magenta case), the systems will stay in a neighborhood of the reference cycle.

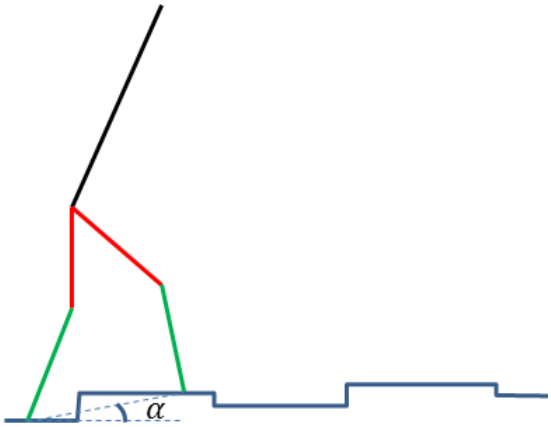

Fig. 11 A simple humanoid walking over uneven terrain. α represents the virtual slope.

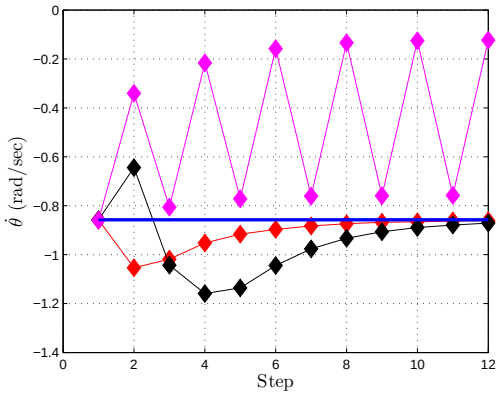

Fig. 12 Poincaré Maps for the system under different virtual slopes, during 12 steps. Blue: nominal cycle (plain ground). Red: Virtual slope of 5° in the first step, 0° for the rest. Black: Virtual slope of −2° for the first step, 10° for the second and 0° for the rest. Magenta: Alternating −5° and 5°.

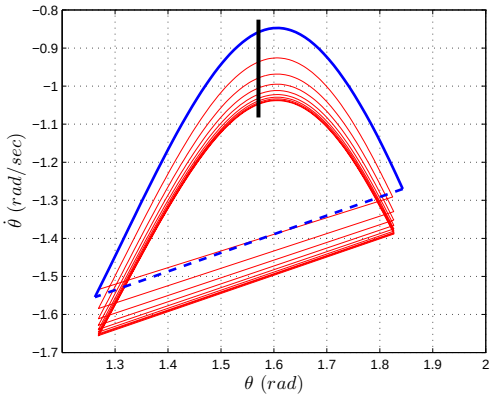

Fig. 13 Phase plane of θ, $\dot{\theta}$ for the introduction of Coulomb friction at the actuated joints. Blue: nominal cycle. Red: actual cycle.

5.4.4 Friction

Another important effect to consider is friction, specially at the knee joints, since the phasing variable θ depends on the behavior of q_2. Therefore, the Coulomb friction vector

$$\mathbf{F} = [F_1, \ldots, F_5]^\top \tag{87}$$

is subtracted to the right side of (58), with

$$F_i = F_i^c \text{sign}(\dot{q}_i), \quad i = 1, \ldots, 5. \tag{88}$$

The numerical tests were performed under an assumption that only the active joints $q_2, \ldots, q_5$ were affected by friction forces, which is why the friction coefficients were selected as $F_2^c = F_5^c = -2.1$, $F_3^c = F_4^c = -1.02$ and $F_1^c = 0$. The results are shown in Fig. 13. Even in the presence of the Coulomb friction, stable walking is still achieved after several steps, as can be seen from the phase plane of θ, where the evolution falls into a new orbit, represented in red.

5.4.5 Imperfect detection of the impact

Due to the practical implementation of the controller, there is an inherent delay between the moment of the impact and the switching of the control law, which won't occur at the same time. The effect that this generates increases as the time step used for implementation increases.

¿From Fig. 14 it can be seen that for a time step small enough, the walking cycle does not suffer an evident deviation from the nominal biped cycle. This deviation is mainly present due to the fact that the controller has not been switched, and the error begins to increase between the time the actual impact happens and the time the control law restarts. This effect becomes more and more evident as the time of detection increases: in Fig. 15, the sample time is increased ten times, so the degradation of the walking cycle becomes evident, but is still in a neighborhood around the nominal cycle, as shown in the figure.

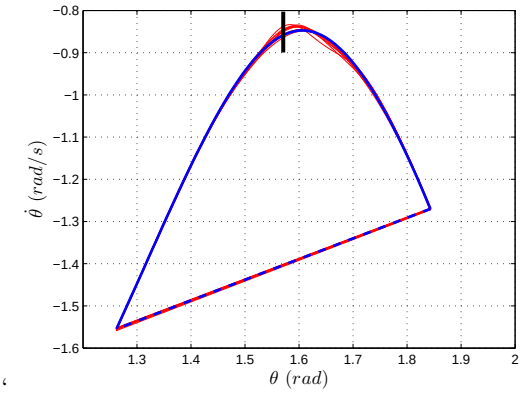

Fig. 14 Phase plane of θ, $\dot{\theta}$ for a time step of 1 ms. Blue: nominal cycle. Red: actual cycle.

5.4.6 External forces and impact disturbances

As shown in Fig. 1, the system was tested under the application of a step disturbance (5 Nm at the hip, along the x axis) during the single support phase, starting from the first step; disturbances at each impact, modifying the impact function Δ in 5% from its original values, were applied as well. The measurements were disturbed by a sinusoidal disburbance of $0.05\sin(2t)$ $rads$, and the initial estimation of the biped velocity is deviated 5% of its designed trajectory's initial velocity.

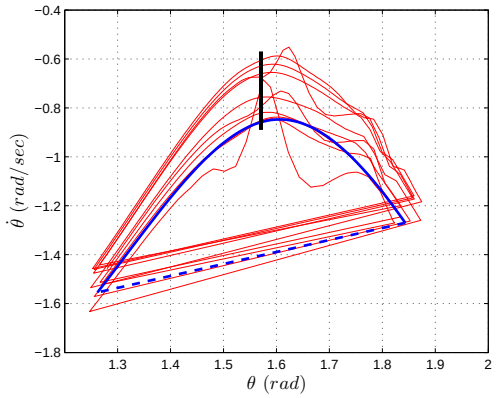

Fig. 15 Phase plane of θ, $\dot{\theta}$ for a time step of 10 ms. Blue: nominal cycle. Red: actual cycle.

Just after the impact, the biggest error amplitude appears due to the disturbance in the impact phase, and this is rapidly attenuated to a lower level, where the new error is due to the disturbance on the continuous dynamics. The new orbit obtained is depicted in Fig. 16 by the red line. Due to the robustness of the controller, this new orbit is close and evolves around the nominal orbit. Even though the evolution of θ does not converge to a limit cycle, due to the effect of the persistent time-varying disturbances, it still remains oscillating in a neighborhood of the nominal cycle. Since the velocity was not measurable, Fig. 17 presents the behavior of the estimator (21) while estimating the missing velocities, where it can be seen that in spite of the persistent time-varying disturbances in the measurements, the error does not diverge.

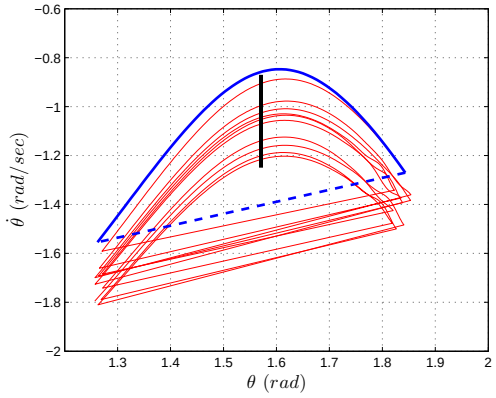

Fig. 16 Phase plane of θ, $\dot{\theta}$ for the disturbed system with persistent perturbations. The blue line represents the limit cycle for the undisturbed system, whereas the red represents the orbit of the system under the perturbations. The black line indicates the Poincaré section.

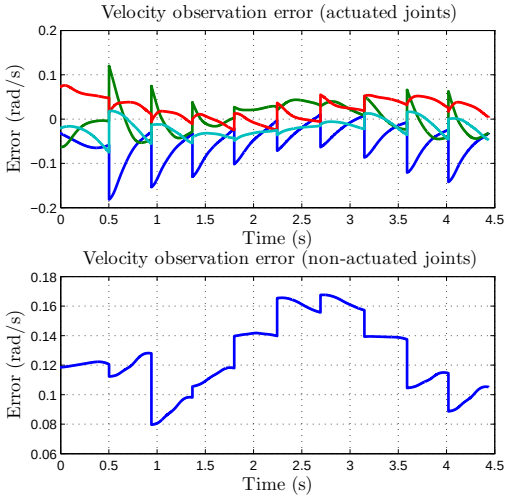

Fig. 17 Velocity estimation errors $\boldsymbol{\xi_2} = (\xi_{21}, \ldots, \xi_{25})^\top$ for the estimator (21), for the disturbed system with persistent perturbations. The estimation error does not diverge under the presence of disturbances in both the measurements and the plant dynamics.

Finally, the previous results were compared against the implementation of a PD-controller, similar to the one presented in the work of Hamed et al (2014). In order to make a fair comparison, the same structure as (4) was used, but $\mathbf{u}$ was replaced with:

$$\dot{\boldsymbol{\xi}} = \mathbf{f}(\boldsymbol{\xi}, t) - \mathbf{g_2}(\boldsymbol{\xi}, t)\mathbf{K}\boldsymbol{\xi} + \mathbf{L}[\mathbf{y} - \mathbf{h_2}(\boldsymbol{\xi}, t)]$$
$$\boldsymbol{\xi}^+ = \boldsymbol{\Delta}(\boldsymbol{\xi}^-, t_i) \tag{89}$$
$$\mathbf{u} = -\mathbf{K}\boldsymbol{\xi} \tag{90}$$

where (89) has the form of a nonlinear Luenberger observer, and (90) of a standard PD-control, with $\mathbf{L}$ and $\mathbf{K} = (\mathbf{K_p}^\top, \mathbf{K_v}^\top)^\top$ constant gain matrices. To obtain the values of both matrices, first the Differential Riccati Equations (16)-(17) are solved along the nominal trajectory $\mathbf{q}_\star$, using the same method and parameters as in Sect. 5.4. Then, the undisturbed closed loop system (1)-(2), (4), (21)-(22) is simulated (with zero initial conditions) for just one step, that ends at time t_1. Thus, the gain matrices $\mathbf{L}$ and $\mathbf{K}$ for the PD-control are calculated as:

$$\mathbf{L} = \frac{1}{t_1}\int_0^{t_1} \mathbf{Z}_\varepsilon(t)\mathbf{C_2}^\top(t)\mathrm{d}t \tag{91}$$

$$\mathbf{K} = \frac{1}{t_1}\int_0^{t_1} \mathbf{B_2}^\top(t)\mathbf{P}_\varepsilon(t)\mathrm{d}t \tag{92}$$

so they become the average values of the time-varying gains of the $\mathcal{H}_\infty$-controller (21)-(22). The transversal control $\mathbf{v}$ in (64) is replaced by $\mathbf{v} = \mathbf{K}_\perp\mathbf{x}_\perp$, and $\mathbf{K}_\perp$ is obtained following the same idea. Once these values are obtained, the system is tested again with the same disturbances as the ones presented at the beginning of this

section, but replacing (21)-(22) with (89)-(90), and the results were compared against the previously exposed.

Figure 18 compares the evolution of the Poincaré maps for both cases. It can be seen that the implementation of the proposed $\mathcal{H}_\infty$-control exhibits better velocity tracking, since its map evolution is closer to the nominal fixed point than in the case of the PD-controller. Also, Fig. 19 compares the cumulative tracking error for both implementations: after three steps, the $\mathcal{H}_\infty$-control performance is better than that of the PD-control, and stays better for successive steps. This is also reflected in the time shifting from the reference trajectory: whereas for the undisturbed case, it takes 5.6 s to complete 10 steps, it took 4.6 s to the $\mathcal{H}_\infty$ implementation, and 3.69 s to the PD implementation, so the behavior of the former is closer to the nominal behavior than that of the latter. Thus, better performance can be concluded for the implementation of the proposed synthesis.

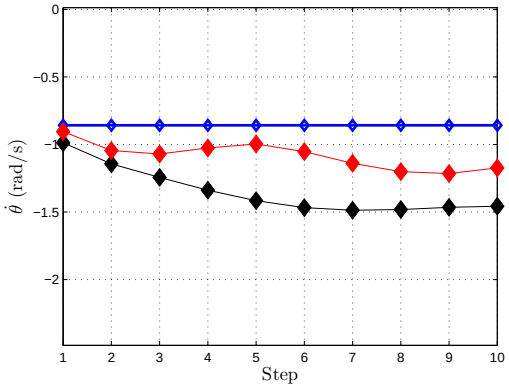

Fig. 18 Comparison of the Poincare Maps for the $\mathcal{H}_\infty$ and PD-controller implementations, for the disturbed system under persistent disturbances. Red: $\mathcal{H}_\infty$. Black: PD; Blue: Nominal behavior

6 Conclusion

The robust $\mathcal{H}_\infty$ output feedback synthesis was developed for underactuated mechanical systems with unilateral constraints. When only imperfect position measurements were available, the synthesis was applied to an underactuated bipedal robot, operating under external disturbances, affecting both the impact-free motion and the transition dynamics. Once a nominal feasible periodic trajectory to follow was prescribed for the bipedal robot, the analysis of the transversal dynamics allowed to carry out sufficient conditions for attenuating the plant disturbances around the prescribed trajectory. The resulting synthesis was tested in the numerical study made for a five-link planar bipedal emulator to be stabilized around a periodic nominal trajectory. Good performance of the closed-loop system was obtained in spite of external disturbances, affecting the single support phase and the impact phase, and under imperfections in the position measurements.

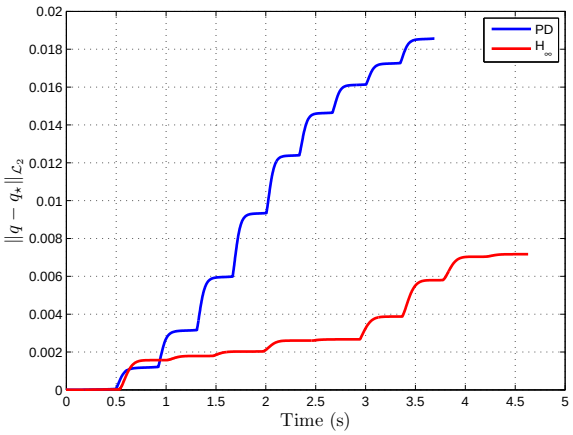

Fig. 19 Comparison of the cumulative tracking errors of the $\mathcal{H}_\infty$ vs PD-controller, for the disturbed system under persistent disturbances.

Acknowledgments

The authors acknowledge the financial support of Campus France grant Eiffel and CONACYT grant no.165958.

References

Alcaraz-Jiménez J, Herrero-Pérez D, Martínez-Barberá H (2013) Robust feedback control of zmp-based gait for the humanoid robot nao. The International Journal of Robotics Research 32(9-10):1074–1088

Ames A, Galloway K, Grizzle J (2012) Control lyapunov functions and hybrid zero dynamics. In: Decision and Control (CDC), 2012 IEEE 51st Annual Conference on, IEEE, pp 6837–6842

Angelosanto G (2008) Kalman filtering of imu sensor for robot balance control. PhD thesis, Massachusetts Institute of Technology

Aoustin Y, Formalsky A (2003) Control design for a biped: reference trajectory based on driven angles as functions of the undriven angle. Journal of Computer and Systems Sciences International 42(4):645–662

Aoustin Y, Chevallereau C, Formalsky A (2006) Numerical and experimental study of the virtual quadrupedal walking robot-semiquad. Multibody System Dynamics 16(1):1–20

Aoustin Y, Chevallereau C, Orlov Y (2010) Finite time stabilization of a perturbed double integrator-part ii: applications to bipedal locomotion. In: Decision and Control (CDC), 2010 49th IEEE Conference on, IEEE, pp 3554–3559

Arai H, Tanie K, Shiroma N (1998) Time-scaling control of an underactuated manipulator. In: Robotics and Automation, 1998. Proceedings. 1998 IEEE International Conference on, IEEE, vol 3, pp 2619–2626

Basar T, Bernhard P (1995) $\mathcal{H}_\infty$-optimal control and related minimax design problems: a dynamic game approach. Boston: Birkhaeuser

Bezier P (1972) Numerical control: Mathematics and applications. Wiley and Sons

Brogliato B (1999) Nonsmooth Mechanics.: Models, Dynamics and Control. Springer

Bullo F, Lynch K (2001) Kinematic controllability for decoupled trajectory planning in underactuated mechanical systems. Robotics and Automation, IEEE Transactions on 17(4):402–412

Chevallereau C, Abba G, Aoustin Y, Plestan F, Westervelt E, Canudas De Wit C, Grizzle J (2003) Rabbit: A testbed for advanced control theory. IEEE Control Systems Magazine 23(5):57–79

Chevallereau C, Grizzle J, Shih C (2009) Asymptotically stable walking of a five-link underactuated 3-d bipedal robot. Robotics, IEEE Transactions on 25(1):37–50

Dai H, Tedrake R (2012) Optimizing robust limit cycles for legged locomotion on unknown terrain. In: Decision and Control (CDC), 2012 IEEE 51st Annual Conference on, IEEE, pp 1207–1213

Dai H, Tedrake R (2013) $\mathcal{L}_2$-gain optimization for robust bipedal walking on unknown terrain. In: Robotics and Automation (ICRA), 2013 IEEE International Conference on, IEEE, pp 3116–3123

Djoudi D, Chevallereau C, Aoustin Y (2005) Optimal reference motions for walking of a biped robot. In: Robotics and Automation, 2005. ICRA 2005. Proceedings of the 2005 IEEE International Conference on, IEEE, pp 2002–2007

Freidovich L, Shiriaev A (2009) Transverse linearization for mechanical systems with passive links, impulse effects, and friction forces. In: Decision and Control, 2009 held jointly with the 2009 28th Chinese Control Conference. CDC/CCC 2009. Proceedings of the 48th IEEE Conference on, IEEE, pp 6490–6495

Freidovich L, Shiriaev A, Manchester I (2008) Stability analysis and control design for an underactuated walking robot via computation of a transverse linearization. In: Proc. 17th IFAC World Congress, Seoul, Korea, pp 10–166

Goebel R, Sanfelice R, Teel A (2009) Hybrid dynamical systems. Control Systems, IEEE 29(2):28–93

Grizzle J, Abba G, Plestan F (2001) Asymptotically stable walking for biped robots: Analysis via systems with impulse effects. Automatic Control, IEEE Transactions on 46(1):51–64

Haddad W, Kablar N, Chellaboina V, Nersesov S (2005) Optimal disturbance rejection control for nonlinear impulsive dynamical systems. Nonlinear Analysis: Theory, Methods & Applications 62(8):1466–1489

Hamed K, Grizzle J (2013) Robust event-based stabilization of periodic orbits for hybrid systems: Application to an underactuated 3d bipedal robot. In: Proceedings of the 2013 American Control Conference

Hamed K, Grizzle J (2014) Event-based stabilization of periodic orbits for underactuated 3-d bipedal robots with left-right symmetry. Robotics, IEEE Transactions on 30(2):365–381

Hamed K, Buss B, Grizzle J (2014) Continuous-time controllers for stabilizing periodic orbits of hybrid systems: Application to an underactuated 3d bipedal robot. Proceedings of the 53rd IEEE Conderence on Decision and Control

Hobbelen D, Wisse M (2007) A disturbance rejection measure for limit cycle walkers: The gait sensitivity norm. Robotics, IEEE Transactions on 23(6):1213–1224

Isidori A, Astolfi A (1992) Disturbance attenuation and $\mathcal{H}_\infty$-control via measurement feedback in nonlinear systems. Automatic Control, IEEE Transactions on 37(9):1283–1293

La Hera P, Shiriaev A, Freidovich L, Mettin U, Gusev S (2013) Stable walking gaits for a three-link planar biped robot with one actuator. Robotics, IEEE Transactions on 29(3):589–601

Leonov G (2006) Generalization of the andronov-vitt theorem. Regular and chaotic dynamics 11(2):281–289

Manamani N, Gauthier N, MSirdi N (1997) Sliding mode control for pneumatic robot leg. In: Proceedings European Control Conference

Mettin U, La Hera P, Freidovich L, Shiriaev A (2007) Planning human-like motions for an underactuated humanoid robot based on the virtual constraints approach. In Proc 13th International Conference on Advanced Robotics, Jeju, Korea, pp 585–590

Meza-Sanchez I, Aguilar L, Shiriaev A, Freidovich L, Orlov Y (2011) Periodic motion planning and nonlinear $\mathcal{H}_\infty$ tracking control of a 3-dof underactuated helicopter. International Journal of Systems Science 42(5):829–838

Miossec S, Aoustin Y (2005) A simplified stability study for a biped walk with underactuated and overactuated phases. The International Journal of Robotics Research 24(7):537–551

Miossec S, Aoustin Y (2006) Dynamical synthesis of a walking cyclic gait for a biped with point feet. In: Fast motions in biomechanics and robotics, Springer, pp 233–252

Montano O, Orlov Y, Aoustin Y (2014) Nonlinear $\mathcal{H}_\infty$-control of mechanical systems under unilateral constraints. In: Proceedings of the 19th World Congress of the International Federation of Automatic Control, IFAC, pp 3833–3838 (extended journal version was submitted to Control Engineering Practice under the title "Nonlinear $\mathcal{H}_\infty$–stabilization of fully actuated bipedal locomotion under unilateral constraints")

Montano O, Orlov Y, Aoustin Y (2015a) Nonlinear output feedback $\mathcal{H}_\infty$-control of mechanical systems under unilateral constraints. Proceedings of the 1st IFAC Conference on Modelling, Identification and Control of Nonlinear Systems pp 284–289

Montano O, Orlov Y, Aoustin Y, Chevallereau C (2015b) Nonlinear orbital $\mathcal{H}_\infty$-stabilization of underactuated mechanical systems with unilateral constraints. Proceedings of the 14th European Control Conference pp 800–805

Morris B, Grizzle J (2005) A restricted poincaré map for determining exponentially stable periodic orbits in systems with impulse effects: Application to bipedal robots. In: Decision and Control, 2005 and 2005 European Control Conference. CDC-ECC'05. 44th IEEE Conference on, IEEE, pp 4199–4206

Naldi R, Sanfelice RG (2013) Passivity-based control for hybrid systems with applications to mechanical systems exhibiting impacts. Automatica 49(5):1104 – 1116

Nešić D, Zaccarian L, Teel A (2008) Stability properties of reset systems. Automatica 44(8):2019–2026

Nešić D, Teel AR, Valmorbida G, Zaccarian L (2013) Finite-gain stability for hybrid dynamical systems. Automatica 49(8):2384 – 2396

Nikkhah M, Ashrafiuon H, Fahimi F (2007) Robust control of underactuated bipeds using sliding modes. Robotica 25(03):367–374

Orlov Y, Aguilar L (2014) Advanced $\mathcal{H}_\infty$ Control–Towards Nonsmooth Theory and Applications. Birkhauser

Orlov Y, Acho L, Solis V (1999) Nonlinear $\mathcal{H}_\infty$-control of time-varying systems. In: Decision and Control, 1999. Proceedings of the 38th IEEE Conference on, IEEE, vol 4, pp 3764–3769

Oza H, Orlov Y, Spurgeon S, Aoustin Y, Chevallereau C (2014) Finite time tracking of a fully actuated biped robot with pre-specified settling time: a second order sliding mode synthesis. In: Robotics and Automation (ICRA), 2014 IEEE International Conference on, IEEE, pp 2570–2575

Raibert M, Tzafestas S, Tzafestas C (1993) Comparative simulation study of three control techniques applied to a biped robot. In: Systems, Man and Cybernetics, 1993.'Systems Engineering in the Service of Humans', Conference Proceedings., International Conference on, IEEE, pp 494–502

Shiriaev A, Perram J, Canudas-de Wit C (2005) Constructive tool for orbital stabilization of underactuated nonlinear systems: Virtual constraints approach. Automatic Control, IEEE Transactions on 50(8):1164–1176

Shiriaev A, Freidovich L, Manchester I (2008) Can we make a robot ballerina perform a pirouette? orbital stabilization of periodic motions of underactuated mechanical systems. Annual Reviews in Control 32(2):200–211

Shiriaev AS, Freidovich LB (2009) Transverse linearization for impulsive mechanical systems with one passive link. Automatic Control, IEEE Transactions on 54(12):2882–2888

Tlalolini D, Chevallereau C, Aoustin Y (2011) Human-like walking: Optimal motion of a bipedal robot with toe-rotation motion. Mechatronics, IEEE/ASME Transactions on 16(2):310–320

Van Der Schaft A (1991) On a state space approach to nonlinear h control. Systems & Control Letters 16(1):1–8

Westervelt E, Buche G, Grizzle J (2004) Experimental validation of a framework for the design of controllers that induce stable walking in planar bipeds. The International Journal of Robotics Research 23(6):559–582

Westervelt E, Grizzle J, Chevallereau C, Choi J, Morris B (2007) Feedback control of dynamic bipedal robot locomotion. CRC press Boca Raton

Westervelt ER, Grizzle JW, Koditschek DE (2003) Hybrid zero dynamics of planar biped walkers. Automatic Control, IEEE Transactions on 48(1):42–56